1

Principle of Low-temperature Fuel Cells Using an Ionic Membrane

Claude Lamy[1,2]

[1]*Université de Montpellier, Institut Européen des Membranes, UMR CNRS no 5635, 2 Place Eugène Bataillon, CC 047, 34095 Montpellier Cedex, France*
[2]*Université de Nantes, Groupe de Recherches HySPàC, CNRS GDR 3652, 2 rue de la Houssinière, 44322 Nantes Cedex 3, France*

1.1 Introduction

A technology-oriented civilization needs more and more energy, particularly the emerging and developing countries. Fossil resources, such as coal, natural gas, and hydrocarbons, are the main primary sources of energy, but they are limited in size and volume and may be exhausted in coming few decades. Moreover, they are the main contributors to carbon dioxide (CO_2) emission that is the principal component of the greenhouse effect. An alternative approach is to use hydrogen (H_2) either to feed fuel cells in power plants, electric vehicles, and electrical devices or to store the intermittent energy (solar, photovoltaic, wind energy, etc.). This approach will strongly limit the production of greenhouse gases (GHGs), depending on the primary sources used for H_2 production since it is not a primary source. Among the renewable energy sources, such as hydroelectric power, wind, solar, and tidal power, the production of H_2 by water (H_2O) electrolysis is the most efficient process, leading to high-purity H_2, which is suitable to feed a low-temperature fuel cell (LTFC), such as a proton exchange membrane fuel cell (PEMFC) or an alkaline fuel cell (AFC) [1–5].

In this context, many investigations were carried out on the development of fuel cells fed either with pure H_2 [3–5] or with other fuels, for example, liquid fuels such as methanol (CH_3OH) [6,7] or ethanol (C_2H_5OH) [5,8]. In particular H_2/O_2 (air) fuel cells, such as PEMFCs, working at relatively low temperatures (ranging from ambient to 70–80 °C), are becoming a mature technology for powering electrical vehicles with an autonomy range approaching 600 km without H_2 refueling or for stationary power plants with relatively good electrical efficiencies (40–55%) depending on the applications and working conditions.

On the other hand, the direct alcohol fuel cell (DAFC), fed with CH_3OH [7] or C_2H_5OH [8], directly converts the chemical energy of alcohol combustion with O_2 into electrical energy. Such devices are particularly suitable for portable electronics, either to recharge their lithium battery or to power them directly. These fuel cells can work either with an acidic electrolyte, such as a proton exchange

Electrocatalysts for Low Temperature Fuel Cells: Fundamentals and Recent Trends, First Edition. Edited by Thandavarayan Maiyalagan and Viswanathan S. Saji.

membrane (PEM), or with a solid alkaline electrolyte, for example, an anion exchange membrane (AEM) in a solid alkaline membrane fuel cell (SAMFC) of similar structure to that of a PEMFC.

In this chapter, we will present the working principle of LTFCs based on the PEM technology, either fed with H_2 (pure H_2 or reformate gases) or with a low-weight alcohol (CH_3OH or C_2H_5OH). Then, we will discuss the electrical energy efficiency either under equilibrium conditions ($j = 0$) or under working conditions at a current density (j), the variation of which with the electrode potential (E), that is, the fuel cell characteristics $E(j)$, will be established from a theoretical analysis of the reaction kinetics. Finally, two typical examples of LTFCs under development and commercialization will be given, the first one concerning the direct methanol fuel cell (DMFC) for portable electronics and the second one the H_2/air PEMFC for the electrical vehicle.

1.2 Thermodynamic Data and Theoretical Energy Efficiency under Equilibrium ($j = 0$)

An elementary fuel cell directly converts the chemical energy of combustion with O_2 of a given fuel (H_2, natural gas, hydrocarbons, kerosene, alcohols, etc.) into electricity (i.e., the Gibbs energy change, $-\Delta G_r$) [6,9–11]. Electrons liberated at the anode (negative pole of the cell) by the electrooxidation of the fuel pass through the external circuit and produce an electrical energy, $W_e = nFE_{cell}$, equal to $-\Delta G_r$, where E_{cell} is the cell voltage, n the number of electrons involved in the overall electrochemical reaction, and $F = 96\,485$ C the Faraday constant (i.e., the electric charge of one electron mole), and reach the cathode (positive pole), where they reduce O_2 (either pure or from air). Inside the fuel cell, the electrical current is transported by migration and diffusion of the electrolyte ions (H^+, OH^-, O^{2-}, and CO_3^{2-}).

1.2.1 Hydrogen/oxygen Fuel Cell

The electrochemical reactions involved in the elementary processes of a H_2/O_2 fuel cell under acidic environment, for example, in a PEMFC (Figure 1.1) are the electrooxidation of H_2 at the anode:

$$H_2 \rightarrow 2H^+ + 2e^- \qquad E_1^0 = 0.000\,\text{V versus SHE} \tag{1.1}$$

and the electroreduction of O_2 at the cathode:

$$1/2\,O_2 + 2H^+ + 2e^- \rightarrow H_2O \qquad E_2^0 = 1.229\,\text{V versus SHE} \tag{1.2}$$

where $E_i^0 = -\Delta G_i^0/(nF)$ is the electrode potential versus the standard hydrogen electrode (SHE) as reference, and ΔG_i^0 is the Gibbs energy change involved in the electrochemical reaction. $\Delta G_i^0 < 0$ since the reactions involved are spontaneous for producing energy.

Similarly, in a fuel cell working in alkaline medium (e.g., an AFC or a SAMFC), the following electrochemical reactions do occur:

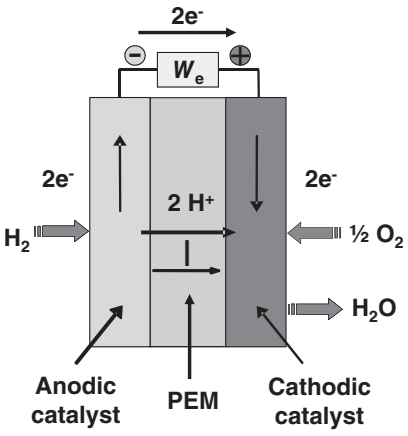

Figure 1.1 Schematic representation of a PEMFC elementary cell showing a PEM on which are pressed the catalytic layers both for the H_2 anode and for the O_2 cathode.

$$H_2 + 2\,OH^- \rightarrow 2\,H_2O + 2\,e^- \qquad \text{at the anode} \tag{1.3}$$

$$1/2\,O_2 + H_2O + 2\,e^- \rightarrow 2\,OH^- \qquad \text{at the cathode} \tag{1.4}$$

In the fuel cell, the electrical balance corresponds to the complete combustion of the fuel in the presence of O_2 as follows:

$$H_2 + 1/2\,O_2 \rightarrow H_2O \tag{1.5}$$

where the thermodynamic data associated with this reaction, under standard conditions ($T = 25\,^{\circ}C$, $p = 1$ bar, and liquid H_2O), have the opposite sign to those of H_2O decomposition:

$$\Delta H^0 = -285.8\ \text{kJ mol}^{-1}\ \text{of}\ H_2 \qquad \text{and}\ \Delta G^0 = -237.2\ \text{kJ mol}^{-1}\ \text{of}\ H_2$$

However, the thermodynamic data to consider (ΔH, ΔG) are those at the working temperature of the device, for example, between 280 and 350 K for the PEMFC and 280–400 K for the AFC (see Table 1.1, where the negative values of the thermodynamic data concern the formation of H_2O, which is a spontaneous process).

The equilibrium cell voltage (E_{eq}) can thus be evaluated from the Nernst potential at each electrode:

$$E_{eq} = E_2 - E_1 = -\Delta G_r/nF = -\Delta G^0/2F + (RT/2F)\text{Ln}\{(p_{H_2})(p_{O_2})1/2/p_{H_2O}\}$$

$$E_{eq} = E^0 + (RT/2F)\text{Ln}\{(p_{H_2})(p_{O_2})1/2/p_{H_2O}\}$$

with $E^0 = -\Delta G^0/2F$ the standard cell voltage, that is, $E^0 = E_2^0 - E_1^0 = 1.229$ V at 25 °C, and p_{H2}, p_{O2}, and p_{H2O} the partial pressures of H_2, O_2, and H_2O, respectively. Therefore, by increasing the pressure of reactants (H_2 and O_2) and decreasing the pressure of the product (H_2O), one can increase the cell voltage.

The variation of E_{eq} with T is contained mainly in the entropic term, that is, $\Delta S^0 = nF\ (dE^0/dT)$, which is the temperature coefficient of the fuel cell. Thus, assuming that ΔH and ΔS are nearly independent of temperature (see Table 1.1), one may calculate E_{eq} as follows:

$$E_{eq}(T) = -\Delta G_r/nF = -(\Delta H - T\,\Delta S)/nF = 1.481 - 0.000846\,T \qquad \text{(in V)}$$

for H_2O in the liquid state at 25 °C ($\Delta H^0 = -285.8\ \text{kJ mol}^{-1}$ and $\Delta S^0 = -163.3\ \text{J mol}^{-1}\ \text{K}^{-1}$).

Table 1.1 Thermodynamic data for the formation of H_2O under a pressure of 1 bar as a function of absolute temperature ($T = 298$–400 K).

H_2O state	T (K)	ΔS (J mol^{-1} K^{-1})	ΔH (kJ mol^{-1})	ΔG (kJ mol^{-1})	E_{eq} (V)	$\varepsilon_{cell}^{rev} = \Delta G/\Delta H$
Liquid	298.15	−163.3	−285.83	−237.17	1.229	0.829
Gaseous	298.15	−44.42	−241.81	−228.57	1.184	0.945
Gaseous	300.00	−44.48	−241.83	−228.49	1.184	0.945
Gaseous	310.00	−44.81	−241.93	−228.04	1.182	0.943
Gaseous	320.00	−45.13	−242.03	−227.59	1.179	0.940
Gaseous	330.00	−45.44	−242.13	−227.14	1.177	0.938
Gaseous	340.00	−45.74	−242.23	−226.68	1.175	0.936
Gaseous	350.00	−46.03	−242.33	−226.23	1.172	0.934
Gaseous	360.00	−46.31	−242.44	−225.76	1.170	0.931
Gaseous	370.00	−46.59	−242.54	−225.30	1.168	0.929
Gaseous	380.00	−46.85	−242.64	−224.83	1.165	0.927
Gaseous	390.00	−47.11	−242.74	−224.36	1.163	0.924
Gaseous	400.00	−47.37	−242.84	−223.89	1.160	0.922

For H_2O in the gaseous state at 25 °C ($\Delta H = -241.8$ kJ mol^{-1} and $\Delta S = -44.42$ J mol^{-1} K^{-1}), one obtains the following:

$$E_{eq}(T) = 1.253 - 0.000230\,T \qquad \text{(in V)}$$

In summary, E_{eq} may be expressed as a function of temperature and pressure (liquid state) by

$$E_{eq}(T,P) = 1.481 - 0.000846\,T + 0.0000431\,T\,\mathrm{Ln}\{(p_{H_2})(p_{O_2})1/2/p_{H_2O}\} \quad \text{in V} \tag{1.6}$$

or

$$E_{eq}(T,P) = 1481 - 0.846\,T + 0.0431\,T\,\mathrm{Ln}\{(p_{H_2})(p_{O_2})1/2/p_{H_2O}\} \quad \text{in mV}$$

In the gaseous state (e.g., at $T = 400$ K with $\Delta H = -242.8$ kJ mol^{-1} and $\Delta S = -47.37$ J mol^{-1} K^{-1}), E_{eq} can be calculated by the following expressions:

$$E_{eq}(T,P) = 1.258 - 0.000245\,T + 0.0000431\,T\,\mathrm{Ln}\{(p_{H_2})(p_{O_2})1/2/p_{H_2O}\} \quad \text{in V} \tag{1.7}$$

or

$$E_{eq}(T,P) = 1258 - 0.245\,T + 0.0431\,T\,\mathrm{Ln}\{(p_{H_2})(p_{O_2})1/2/p_{H_2O}\} \quad \text{in mV}$$

A fuel cell working under reversible thermodynamic conditions (i.e., at equilibrium with $j = 0$) does not follow Carnot's theorem, which controls the energy efficiency of an internal combustion engine (ICE), so the theoretical energy efficiency of an elementary cell, ε_{cell}^{rev}, defined as the ratio of the electrical energy produced

($W_e = nFE_{cell} = -\Delta G_r$) to the chemical energy of combustion ($-\Delta H$), that is,

$$\varepsilon_{cell}^{rev} = -\Delta G/(-\Delta H) = \Delta G/\Delta H = (\Delta H - T\Delta S)/\Delta H = 1 - T(\Delta S/\Delta H) = 1 + T\Delta S/(-\Delta H) \tag{1.8}$$

which can be very high (if $T|\Delta S| \ll |\Delta H|$).

In the case of a H_2/O_2 fuel cell working at 25 °C, the energy efficiency of an elementary cell will be $\varepsilon_{cell}^0 = \Delta G^0/\Delta H^0 = 237.17/285.83 = 0.829 \approx 83\%$, if ΔH is taken with H_2O in the liquid state (standard conditions), that is, ΔH is the high heating value (ΔH_{HHV}). But the heat of H_2O condensation $\Delta Q_{cond} = \Delta H_{HHV} - \Delta H_{LHV} = 285.8 - 241.8 = 44\ kJ\ mol^{-1}$ (where ΔH_{LHV} = low heating value = 241.8 kJ mol^{-1} – see Table 1.1) is not useful for producing electrical energy, so a more realistic energy efficiency will be $\varepsilon_{cell}^{rev} = \Delta G/\Delta H = 228.6/241.8 = 0.945 \approx 95\%$ using the thermodynamic data of H_2O formation under the gaseous state at 25 °C (Table 1.1). On the other hand, using the Gibbs energy change ΔG_r^0, given in Table 1.1, allows us to evaluate the specific energy W_s of H_2 (expressed in kWh kg^{-1}) as follows:

$$W_s = \frac{W_e}{3600\,M} = \frac{(-\Delta G_r^0)}{3600\,M} \tag{1.9}$$

with $M = 0.002$ kg the molecular mass of H_2. This gives

$$W_s = \frac{237.2 \times 10^3}{3600 \times 0.002} = 32.94\ \text{kWh kg}^{-1} \approx 33\ \text{kWh kg}^{-1}$$

which is a very high value when not taking into account the weight of the H_2 tank.

1.2.2 Direct Alcohol Fuel Cell

The DAFC directly converts the Gibbs energy of combustion of an alcohol into electricity, without a fuel processor. This greatly simplifies the system, reducing its volume and cost [12,13]. Important developments of DAFCs are due to the use of a PEM as electrolyte, instead of a liquid acid electrolyte, as previously done.

The electrical energy $W_e = nFE_{cell} = -\Delta G_r$ is related to the Gibbs energy change, ΔG_r, of the oxidation reaction of an alcohol with O_2. The overall combustion reaction of a monoalcohol C_xH_yO leading to H_2O and CO_2, that is,

$$C_xH_yO + \left(x + \frac{y}{4} - \frac{1}{2}\right)O_2 \rightarrow x\,CO_2 + \frac{y}{2}H_2O \tag{1.10}$$

involves the participation of H_2O or of its adsorbed residue (OH_{ads}) provided by the cathodic reaction (electroreduction of dioxygen).

The electrochemical oxidation of a monoalcohol in acid medium to reject the CO_2 produced can thus be written as follows:

$$C_xH_yO + (2x - 1)H_2O \rightarrow x\,CO_2 + n\,H^+ + n\,e^- \tag{1.11}$$

with $n = 4x + y - 2$. Such an anodic reaction is very complicated from a kinetics point of view since it involves multielectron transfers and the presence of different adsorbed intermediates and several reaction products and by-products (see Section 3.3.4 in Chapter 3). However, from the thermodynamic data it is easy

to calculate the standard equilibrium potential, E^0_{eq}, the theoretical efficiency and the energy density under standard conditions.

According to reaction (1.11), the standard Gibbs energy change, ΔG^0_1, allowing to calculate the standard anode potential $E^0_1 = -\Delta G^0_1/nF$, can be evaluated from the standard energy of the formation ΔG^f_i of reactant (i):

$$-\Delta G^0_1 = x\Delta G^f_{CO_2} - \Delta G^f_{C_xH_yO} - (2x-1)\Delta G^f_{H_2O} \tag{1.12}$$

In the cathodic compartment, the electroreduction of O_2 does occur as follows:

$$1/2\,O_2 + 2\,H^+ + 2e^- \rightarrow H_2O \tag{1.13}$$

with $\Delta G^0_2 = \Delta G^f_{H_2O} = -237.2$ kJ mol^{-1}, leading to a standard cathodic potential E^0_2:

$$E^0_2 = -\frac{\Delta G^0_2}{2F} = \frac{237.2 \times 10^3}{2 \times 96485} = 1.229\ \text{V versus SHE} \tag{1.14}$$

The standard Gibbs energy change, ΔG^0_r, of the overall reaction (1.10) can be evaluated as follows:

$$\Delta G^0_r = \left(2x + \frac{y}{2} - 1\right)\Delta G^0_2 - \Delta G^0_1 = x\Delta G^f_{CO_2} + \frac{y}{2}\Delta G^f_{H_2O} - \Delta G^f_{C_xH_yO}, \tag{1.15}$$

leading to E^0_{eq} under standard conditions:

$$E^0_{eq} = -\frac{\Delta G^0_r}{nF} = -\left(\frac{\Delta G^0_2}{2F} - \frac{\Delta G^0_1}{nF}\right) = E^0_2 - E^0_1 \tag{1.16}$$

Then, it is possible to evaluate the specific energy W_s in kWh kg^{-1}, using equation (1.9) where M is the molecular mass of the alcohol, and knowing the enthalpy of formation ΔH^f_i from the thermodynamic data, one may calculate ΔH^0_r

$$\Delta H^0_r = \left(2x + \frac{y}{2} - 1\right)\Delta H^0_2 - \Delta H^0_1 = x\,\Delta H^f_{CO_2} + \frac{y}{2}\Delta H^f_{H_2O} - \Delta H^f_{C_xH_yO} \tag{1.17}$$

and the reversible energy efficiency under standard conditions $\varepsilon^0_{cell} = (\Delta G^0_r/\Delta H^0_r)$.

For example, for CH_3OH and C_2H_5OH, the electrochemical oxidation reactions and the standard anode potentials are, respectively, as follows:

$$CH_3OH + H_2O \rightarrow CO_2 + 6\,H^+ + 6\,e^- \quad E^{0\ MeOH}_{cell} = 0.016\ \text{V versus SHE} \tag{1.18}$$

$$CH_3CH_2OH + 3\,H_2O \rightarrow 2\,CO_2 + 12\,H^+ + 12\,e^- \quad E^{0\ EtOH}_{cell} = 0.084\ \text{V versus SHE} \tag{1.19}$$

This corresponds to the overall combustion reaction of these alcohols in O_2:

$$CH_3OH + 3/2\,O_2 \rightarrow CO_2 + 2\,H_2O \tag{1.20}$$

$$CH_3CH_2OH + 3\,O_2 \rightarrow 2\,CO_2 + 3\,H_2O \tag{1.21}$$

with the thermodynamic data under standard conditions (see Table 1.2). The corresponding E^0_{eq} are the following:

Table 1.2 Thermodynamic data associated with the electrochemical oxidation of some alcohols under standard conditions (25 °C, 1 bar, and liquid phase).

Alcohol	ΔG_1^0 (kJ mol^{-1})	E_1^0 (V) versus SHE	ΔG_r^0 (kJ mol^{-1})	E_{cell}^0 (V)	W_s (kWh kg^{-1})	ΔH_r^0 (kJ mol^{-1})	ε_{cell}^0
CH_3OH	−9.3	0.016	−702	1.213	6.09	−726	0.967
C_2H_5OH	−97.3	0.084	−1326	1.145	8.00	−1367	0.969
C_3H_7OH	−171	0.098	−1963	1.131	9.09	−2027	0.968
1-C_4H_9OH	−409	0.177	−2436	1.052	9.14	−2676	0.910
CH_2OH–CH_2OH	−25.5	0.026	−1160	1.203	5.20	−1189	0.976
CH_2OH–$CHOH$–CH_2OH	1	−0.001	−1661	1.230	5.02	−1650	1.01

$$E_{cell}^{0\ MeOH} = -\frac{\Delta G_r^0}{6F} = -\frac{\Delta G_2^0}{2F} + \frac{\Delta G_1^0}{6F} = E_2^0 - E_1^{0\ MeOH} = 1.229 - 0.016 = 1.213\ V$$

$$E_{cell}^{0\ EtOH} = -\frac{\Delta G_r^0}{12F} = -\frac{\Delta G_2^0}{2F} + \frac{\Delta G_1^0}{12F} = E_2^0 - E_1^{0\ EtOH} = 1.229 - 0.084 = 1.145\ V$$

For higher alcohols, such as *n*-propanol, for example, the following calculations can be made:

$$C_3H_7OH + 5\,H_2O \rightarrow 3\,CO_2 + 18\,H^+ + 18\,e^- \tag{1.22}$$

$$-\Delta G_1^0 = 3\,\Delta G_{CO_2}^f - \Delta G_{C_3H_7OH}^f - 5\,\Delta G_{H_2O}^f = -3 \times 394.4 + 168.4 + 5 \times 237.1 = 171\ kJ\ mol^{-1}$$

$$\text{so that } E_1^0 = -\frac{\Delta G_1^0}{18F} = \frac{171 \times 10^3}{18 \times 96485} = 0.098\ V \text{ versus SHE}$$

and

$$C_3H_7OH + 9/2\,O_2 \rightarrow 3\,CO_2 + 4\,H_2O \tag{1.23}$$

with

$$\Delta G_r^0 = 9\Delta G_2^0 - \Delta G_1^0 = 3\Delta G_{CO_2}^f + 4\Delta G_{H_2O}^f - \Delta G_{C_3H_7OH}^f$$
$$= -3 \times 394.4 - 4 \times 237.1 + 168.4 = -1963\ kJ\ mol^{-1}$$

E_{eq}^0 under standard conditions is thus

$$E_{eq}^0 = -\frac{\Delta G_r^0}{18F} = \frac{1963 \times 10^3}{18 \times 96485} = \frac{237.1 \times 10^3}{2 \times 96485} - \frac{171 \times 10^3}{18 \times 96485} = 1.229 - 0.098 = 1.131\ V$$

and the specific energy is

$$W_s = \frac{1963 \times 10^3}{3600 \times 0.060} = 9.09\ kWh\ kg^{-1}$$

The enthalpy change of reaction (1.23) is

$$\Delta H_r^0 = -3 \times 395.5 - 4 \times 285.8 + 302.6 = -2027\ kJ\ mol^{-1}$$

so the reversible energy efficiency under standard condition is

$$\varepsilon_{cell}^0 = \frac{\Delta G_r^0}{\Delta H_r^0} = \frac{1963}{2027} = 0.968 \approx 97\%$$

For all the alcohols listed in Table 1.2, E^0_{cell}varies from 1.23 to 1.05 V, which is very similar to that of a H_2/O_2 fuel cell ($E^0_{cell} = 1.229$ V). The energy density varies from 0.5 to 1 of that of gasoline (which is around 10–11 kWh kg^{-1}); therefore, these compounds are good alternative fuels to hydrocarbons. Furthermore, the reversible energy efficiency ε^0_{cell} is close to 1, while that of the H_2/O_2 fuel cell is 0.83 at 25 °C (standard conditions).

1.3 Electrocatalysis and the Rate of Electrochemical Reactions

However, under working conditions, the practical electric efficiency of a fuel cell depends on the current density j that is delivered by the cell and is lower than that of the equilibrium reversible efficiency (at $j = 0$). This is due to the irreversibility of the electrochemical reactions involved at the electrodes, leading to overpotentials η_a at the anode, η_c at the cathode, so the working E_{cell} becomes (taking into account the ohmic losses R_e j coming from the cell resistance R_e)

$$E_{cell}(j) = E^0_{eq}(j = 0) - (|\eta_a| + |\eta_c| + R_e|j|) \tag{1.24}$$

where the overpotentials η_i are defined as the deviation of the working electrode potential $E_i(j)$ from the equilibrium potential $E^{(i)}_{eq}(0)$ [14–16]; that is, $\eta_i = E_i(j) - E^{(i)}_{eq}(0)$.

For the H_2 electrode, η_a is very small and can be approximated by a linear relationship with j, that is, $\eta_a = R_t\, j$, where R_t is the charge transfer resistance (see Section 1.3.1). But for the alcohol oxidation, η_a is at least 0.3–0.4 V for a reasonable j value (100 mA cm^{-2}), so E_{cell}, including an overpotential $\eta_c = -0.3$ to -0.4 V for the cathodic reaction, will be on the order of 0.4–0.6 V, and the voltage efficiency will be $\varepsilon_E = E_{cell}(j)/E^0_{eq} = (0.4/1.2 = 0.33)$ to $(0.6/1.2 = 0.50)$, under operating conditions. Such a drawback of the direct alcohol fuel cell can be removed only by improving the kinetics of the electrooxidation of the fuel. This needs to have a relative good knowledge of the reaction mechanisms, particularly of the rate determining step, and to search for electrode materials (Pt-X binary and Pt-X-Y ternary electrocatalysts) with improved catalytic properties (see Chapter 3, Section 3.3.4).

From Eq. (1.24), it follows that the increase in the practical fuel cell efficiency ε_{cell} can be achieved by increasing the voltage efficiency $\varepsilon_E = E_{cell}(j)/E^0_{eq}$ and the Faradaic efficiency $\varepsilon_F = n_{exp}/n_{th}$, the reversible efficiency, ε^{rev}_{cell}, being fixed by the thermodynamic data under the working conditions (temperature and pressure) (see Eq. (1.38).

For a given electrochemical system, the increase in voltage efficiency is directly related to the decrease in overpotentials of the oxygen reduction reaction (ORR), $|\eta_c|$, and alcohol oxidation reaction, η_a, which needs to enhance the activity of the catalysts at low potentials and low temperatures, whereas the increase in Faradaic efficiency is related to the ability of the catalyst to oxidize completely, or not, the fuel into CO_2, that is, it is related to the selectivity of the catalyst. Indeed, in the case of C_2H_5OH, for example, acetaldehyde and acetic acid are formed at the anode [17],

which corresponds to a number of electrons involved, 2 and 4, respectively, against 12 for the complete oxidation of C_2H_5OH to CO_2. The enhancement of both these efficiencies is a challenge in electrocatalysis.

In the following section, we will evaluate the different overvoltages involved in an elementary fuel cell and establish the electrical characteristics $E_{cell}(j)$ of the cell.

1.3.1 Establishment of the Butler–Volmer Law (Charge Transfer Overpotential)

For a given electrochemical reaction $A + n\ e^- \leftrightarrow B$, which involves the transfer of n electrons at the electrode–electrolyte interface, the equilibrium potential (at $j = 0$), called the electrode potential, is given by the Nernst law as follows:

$$E_{eq}^{A/B} = E_0^{A/B} + \frac{RT}{nF} \mathrm{Ln} \frac{a_A}{a_B} \tag{1.25}$$

where $E_0^{A/B}$ is the standard electrode potential versus SHE (whose potential is zero at 25 °C by definition), and a_i the activity of reactant (i). As soon as the electrode potential takes a value $E^{A/B}$ different from the equilibrium potential, $E_{eq}^{A/B}$, an electrical current of intensity I passes through the interface, whose magnitude depends on the deviation $\eta = E^{A/B} - E_{eq}^{A/B}$ from the equilibrium potential. η, which is called the overpotential, is positive for an oxidation reaction (anodic reaction $B \rightarrow A + n\ e^-$) and negative for a reduction reaction (cathodic reaction $A + n\ e^- \rightarrow B$). The current intensity I is proportional to the rate of reaction (r), that is, $I = nFr$. For a heterogeneous reaction, r is proportional to the surface area S of the interface, so the kinetics of electrochemical reactions is better defined by the intrinsic rate $r_i = r/S$ and the current density $j = I/S = nFr_i$.

The electrical characteristics $j(E)$ can then be obtained by introducing the exponential behavior of the rate constant (Arrhenius law) with the electrochemical activation energy, $\Delta\overline{G}^+ = \Delta G_0^+ - \alpha\, n\, F\, E$, which comprises two terms: the first one (ΔG_0^+) is the chemical activation energy and the second one (αnFE) is the electrical component of the activation energy. The latter is a fraction α ($0 \le \alpha \le 1$) of the total electric energy, nFE, coming from the applied electrode potential E, where α is called the charge transfer coefficient. The chemical activation energy can be decreased by a factor K coming from the presence of a catalytic material in the electrode structure, so electrocatalysis can be defined as the activation of electrochemical reactions both by the electrode potential and by the electrode material (Figure 1.2).

In the theory of absolute reaction rate, one obtains for a first-order electrochemical reaction, the rate of which is proportional to the concentration c_i of reactant (i) [18],

$$r_a = k_a(E,T) S\, c_B^{elec} = k_a^0\, S\, c_B^{elec} \exp(-\Delta\overline{G}_a^+/RT) \quad \text{with } \Delta\overline{G}_a^+ = \Delta G_a^+ - (1-\alpha)\, nFE$$

$$r_c = k_c(E,T) S\, c_A^{elec} = k_c^0\, S\, c_A^{elec} \exp(-\Delta\overline{G}_c^+/RT) \quad \text{with } \Delta\overline{G}_c^+ = \Delta G_c^+ + \alpha\, nFE$$

where c_i^{elec} is the concentration of reactant (i) at the electrode surface and α is the charge transfer coefficient ($0 < \alpha < 1$), that is, the fraction of the electrical energy that activates the reduction reaction ($A \rightarrow B$), and $(1-\alpha)$ nFE activating the oxidation reaction ($B \rightarrow A$). Thus, $I = nF(r_a - r_c)$ so that $j = I/S$, that is, the current

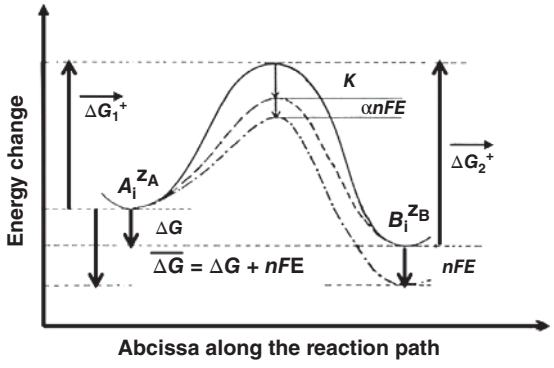

Figure 1.2 Activation barrier for an electrochemical reaction. *K* is the decrease in activation energy due to the electrode catalyst and *αnFE* is that due to the electrode potential *E*.

intensity I divided by the electrode surface area S, is given by

$$j = I/S = nF[\mathrm{k}_\mathrm{a}^0\, c_\mathrm{B}^\mathrm{elec} \exp(-\Delta G_\mathrm{a}^+/RT)\exp[(1-\alpha)nFE/RT] - k_\mathrm{c}^0\, c_\mathrm{A}^\mathrm{elec} \exp(-\Delta G_\mathrm{c}^+/RT)\exp[-\alpha nFE/RT]$$

where the indices "a" or "c" stands for the anodic or cathodic reaction, respectively, and k_i are the corresponding rate constant.

∗At equilibrium $j = 0$ and $r_\mathrm{a} = r_\mathrm{c}$, so that $j_\mathrm{a} = -j_\mathrm{c} = j_0$, $E = E_\mathrm{eq}$, and $c_i^\mathrm{elec} = c_i^0$, where c_i^0 is the bulk concentration of reactant (i). This gives

$$j_0 = nFk_\mathrm{a}^0 c_\mathrm{B}^0 \exp(-\Delta G_\mathrm{a}^{+0}/RT)\exp[(1-\alpha)nFE_\mathrm{eq}/RT] = nFk_\mathrm{c}^0 c_\mathrm{A}^0 \exp(-\Delta G_\mathrm{c}^{+0}/RT)\exp(-\alpha nF\, E_\mathrm{eq}/RT)$$

leading to $j_0 = nF(k_\mathrm{c}^0)^{1-\alpha}(k_\mathrm{a}^0)^\alpha(c_\mathrm{A}^0)^{1-\alpha}(c_\mathrm{B}^0)^\alpha = nF\, k_\mathrm{s}^0(c_\mathrm{A}^0)^{1-\alpha}(c_\mathrm{B}^0)^\alpha$.

j_0 is called the exchange current density and k_s^0 the standard rate constant. Then,

$$E_\mathrm{eq}^\mathrm{A/B} = E_0^\mathrm{A/B} + RT/nF\ \mathrm{Ln}(c_\mathrm{A}^0/c_\mathrm{B}^0) = E_0^\mathrm{A/B} + RT/nF\ \mathrm{Ln}(K_\mathrm{eq})$$

where the activity a_i of reactant (i) has been replaced by its concentration c_i, K_eq is the equilibrium constant of reaction $\mathrm{A} + n\ \mathrm{e}^- \leftrightarrow \mathrm{B}$ and $E_0^\mathrm{A/B} = \exp(-\Delta G_\mathrm{r}^0/RT)$ is the standard electrode potential, with $\Delta G_\mathrm{r}^0 = \Delta G_\mathrm{a}^{+0} - \Delta G_\mathrm{c}^{+0}$ the Gibbs energy of reaction.

This corresponds to the *Nernst law*.

∗Out of equilibrium $j = j_\mathrm{a} + j_\mathrm{c} \neq 0$ and dividing j by j_0 one obtains

$$j(\eta) = j_0[(c_\mathrm{B}^\mathrm{elec}/c_\mathrm{B}^0)\exp\{(1-\alpha)(nF/RT)\eta\} - (c_\mathrm{A}^\mathrm{elec}/c_\mathrm{A}^0)\exp\{-\alpha(nF/RT)\eta\}] \tag{1.26}$$

or $j(\eta) = j_0[\exp\{(1-\alpha)(nF/RT)\eta\} - \exp\{-\alpha(nF/RT)\eta\}]$

when assuming no mass transfer limitation, that is, $c_\mathrm{i}^\mathrm{elec} = c_\mathrm{i}^0$.

This is the *Butler–Volmer law* with $\eta = E - E_\mathrm{eq}$ the overpotential and j_0 the exchange current density.

The expression of the Butler–Volmer law can be simplified in some limiting cases:

i) For $|\eta| \ll RT/nF$ ($\approx 25.7/n$ mV at 25 °C) then $j(\eta) = j_0\ (nF/RT)\ \eta = \eta/R_\mathrm{t}$

or

$$\eta = R_t\, j \text{ with } R_t = RT/(nFj_0) \text{ the charge transfer resistance.} \tag{1.27}$$

This is the *Ohm's law*.

ii) For $\eta \gg RT/nF$ then $j(\eta) = j_0 \exp\{(1-\alpha)\ (nF/RT)\ \eta\}$ or $\eta = RT/\{(1-\alpha)\ nF)\}$ Ln (j/j_0) (with $j > 0$),
and for $\eta \ll -RT/nF$, then $j(\eta) = -j_0 \exp\{-\alpha(nF/RT)\ \eta\}$ or $\eta = -RT/(\alpha\ nF)$ Ln $(-j/j_0)$ (with $j < 0$),
that is,

$$\eta = a \pm b_i \log_{10}|j| \tag{1.28}$$

This is the *Tafel law* with the Tafel slopes $b_i = 2.3\ RT/(\alpha_i nF)$ in V $dec^{-1} \approx 59/(\alpha_i n)$ mV at 25 °C and $\alpha_i = \alpha_a$ for an oxidation reaction and $\alpha_i = \alpha_c$ for a reduction reaction. For a simple electrochemical reaction $\alpha_a + \alpha_c = 1$.

iii) For the hydrogen oxidation reaction (HOR) j_0 is very high ($j_0 \approx 1$ mA cm^{-2}) so that the reaction is reversible and the Ohm's law does apply; therefore, a linear relationship between η and j is obtained, that is, $j(\eta) = \eta/R_t$.

iv) For the ORR j_0 is small ($j_0 \approx 1$ μA cm^{-2}) so that the reaction is irreversible (one may neglect the reverse reaction, i.e., H_2O oxidation) and one may write:

$$j(\eta) = -\,j_0 \exp\{-\alpha_c(nF/RT)\eta\} \quad \text{or } \eta_c^{act} = -RT/(\alpha_c\ nF)\mathrm{Ln}(|j|/j_0)$$

where η_c^{act} is the activation overpotential for an irreversible reaction, such as the ORR or the alcohol oxidation reaction (AOR), with j_0 given by

$$j_0 = nFk_a^0 c_B^0 \exp(-\Delta G_a^{+0}/RT)\exp(\alpha_a\ nF\ E_{eq}/RT) = nFk_c^0 c_A^0 \tag{1.29}$$
$$\exp(-\Delta G_c^{+0}/RT)\exp(-\alpha_c nF\ E_{eq}/RT)$$

with α_a, α_c the charge transfer coefficients for the anodic or the cathodic reaction, respectively. $\alpha_c = 1 - \alpha_a$ usually for an elementary electrochemical reaction.

This last equation contains the two essential activation terms met in electrocatalysis: (i) an exponential function of the electrode potential E and (ii) an exponential function of the chemical activation energy ΔG^{+0}. By modifying the nature and structure of the electrode material, one may decrease ΔG^{+0} by a given amount K (see Figure 1.2), thus increasing j_0, as the result of the catalytic properties of the electrode. This leads to an increase in the reaction rate r_i, that is, of $j = nFr_i$.

1.3.2 Mass Transfer Limitations (Concentration Overpotential)

The reaction kinetics can be controlled by mass transfer (diffusion, migration, and convection) of the reacting species inside the electrolytic phase, so the limiting current density (j_i) is proportional to the mass flux density J_i of species (i): $j_i = |z_i|F J_i$ with $J_i = (1/S)\ (\Delta N_i/\Delta t) = c_i\ v_i$ (where z_i is the algebraic ionic charge of species (i), ΔN_i the number of moles exchanged, v_i the geometric velocity, and S the electrode surface area).

J_i can be expressed by the Nernst–Planck equation:

$$\vec{J}_i = -\frac{D_i c_i}{RT}\vec{\nabla}\overline{\mu}_i + c_i\vec{v}_i^{\,ext} = -D_i\vec{\nabla}c_i - \frac{z_i F}{RT}D_i c_i\vec{\nabla}\varphi + c_i\vec{v}_i^{\,ext} \tag{1.30}$$

with D_i the diffusion coefficient of species (i), $\overline{\mu}_i = \mu_i + z_i F\,\varphi$ its electrochemical potential, and φ the electrode potential, that is, the difference of inner potential at the electrode–electrolyte interface.

In the following, we will neglect the contribution of the convection current $\vec{j}_i^{\,\mathrm{cv}} = |z_i|F\,c_i\,\vec{v}_i^{\,\mathrm{ext}}$ and of the migration current $\vec{j}_i^{\,\mathrm{m}} = |z_i|\,Fu_i\,c_i\,\vec{E} = |z_i|\lambda_i\,c_i\,\vec{E} = \chi_i\,\vec{E}$ where $\lambda_i = Fu_i$ is the molar conductivity with $u_\mathrm{i} = z_i\mathrm{F}D_i/(RT)$ the electric mobility, $\chi_i = |z_i|\,\lambda_i\,c_i$ is the ionic conductivity, and $\vec{E} = \vec{\nabla}\varphi$ the electrical field [19].

Thus, we will consider only the diffusion process (*Fick's laws*) of species (i):

$$\begin{aligned} \vec{J}_i^{\,\mathrm{d}} &= -D_i\,\vec{\nabla}c_i \quad \text{(Fick's 1st law)} \quad \text{and } \vec{j}_i^{\,\mathrm{d}} = |z_i|F\,\vec{J}_i^{\,\mathrm{d}} \\ \frac{\partial c_i}{\partial t} &= -\mathrm{div}\,\vec{J}_i^{\,\mathrm{d}} = D_i\,\Delta c_i \quad \text{(Fick's 2nd law} \approx \text{mass conservation)} \end{aligned} \tag{1.31}$$

The resolution of Fick's equations in the approximation of a semi-infinite linear diffusion, under steady-state conditions, leads to the following relations:

$$\begin{aligned} J_\mathrm{i}^\mathrm{d} &= -D_i\,\partial c_i(x,t)/\partial x,\, \partial c_i(x,t)/\partial t = 0 \quad \text{and } j_i^\mathrm{d} = \pm\,|z_i|F\,D_i|\partial c_\mathrm{i}(x,t)/\partial x|_{x=0} \\ \partial c_\mathrm{i}(x,t)/\partial t &= D_i\,\partial^2 c_i(x,t)/\partial x^2 = 0 \text{ giving } (\partial c_i/\partial x) = \frac{c_{i\mathrm{o}} - c_i(0)}{\delta}, \quad \text{and} \\ c_i(x) &= (\partial c_i/\partial x)_{x=0}\,x + c_i(0) = \frac{c_{i\mathrm{o}} - c_i(0\,)}{\delta}x + c_i(0) \quad (0 \le x \le \delta) \end{aligned}$$

where δ is the thickness of the diffusion layer, $c_{\boldsymbol{i}}(0)$ the concentration at the electrode surface, and $c_{i\mathrm{o}}$ the bulk concentration of reactant (i) (Figure 1.3). For the electrochemical reaction, $\mathrm{A}_i^{z_\mathrm{A}} + ne^- \leftrightarrow \mathrm{B}_i^{z_\mathrm{B}}$, the rate of which is controlled only by diffusion, j can be written as follows:

$$|j| = |j_i^\mathrm{d}| = nF\,D_i(|c_{\mathbf{io}} - c_\mathbf{i}(0)|/\delta), \text{ with } n = z_\mathrm{A} - z_\mathrm{B} \text{ (charge conservation)}$$

For high rate, that is, high current densities, all the reacting species arriving at the electrode surface are immediately consumed, that is, $c_{\boldsymbol{i}}(0) \to 0$, and their activity (concentration) becomes 0. Thus, the concentration gradient reaches a maximum value, leading to the following expression of the limiting current density $j_{\mathrm{l}i}$:

$$j_{\mathrm{l}i} = nF\,D_i\,c_{\mathrm{io}}/\delta \tag{1.32}$$

with D_i (in $\mathrm{m^2\ s^{-1}}$ or $\mathrm{cm^2\ s^{-1}}$) the diffusion coefficient of species (i), $c_{\mathbf{io}}$ its concentration in the bulk of electrolyte, and δ the thickness of the diffusion layer (in the approximation of a semi-infinite linear diffusion).

By doing the ratio of j with $j_{\mathrm{l}i}$ one may obtain the following:

$$|j|/j_{\mathrm{l}i} = [c_{i\mathrm{o}} - c_i(0)]/c_{i\mathrm{o}} = 1 - c_i(0)/c_{i\mathrm{o}} = 1 - p_i(0)/p_{i\mathrm{o}}$$

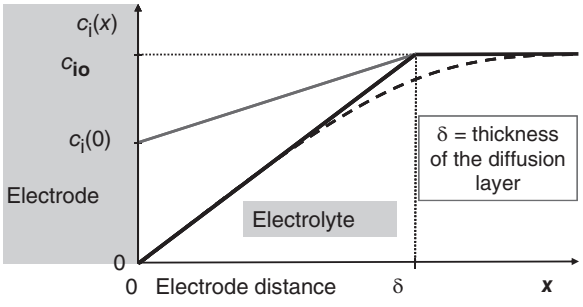

Figure 1.3 Concentration profiles of the reacting species for a semi-infinite linear diffusion under steady-state conditions.

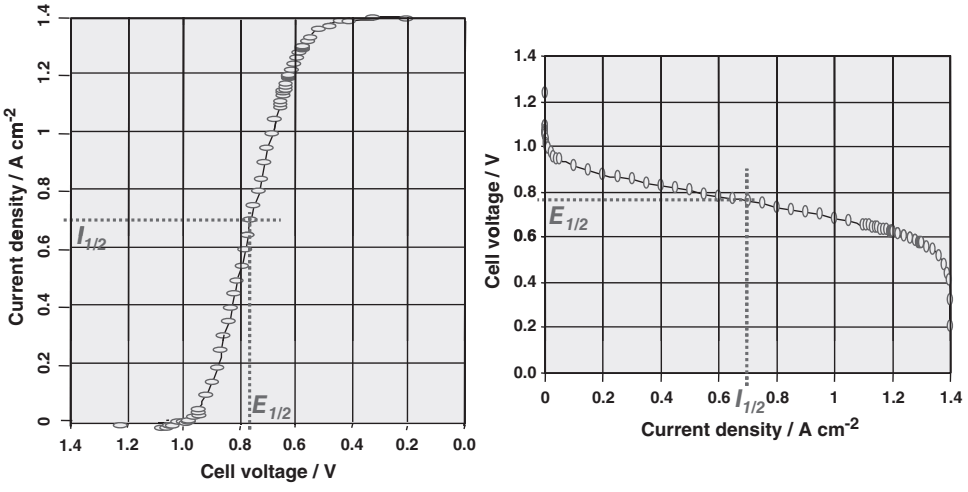

Figure 1.4 Simulation of the $j(E)$ and $E(j)$ curves limited by mass transfer (diffusion) with the following parameters: Tafel slope $b_c = 60\ \text{mV dec}^{-1}$; $j_{la} = 0.0\ \text{A cm}^{-2}$; and $j_{lc} = 1.4\ \text{A cm}^{-2}$.

The surface concentration $c_i(0)$ (or partial pressure $p_i(0)$ for gaseous species) will be given by

$$c_i(0)/c_{io} = p_i(0)/p_{io} = 1 - |j|/j_{li} \tag{1.33}$$

For a very fast transfer reaction ($j_0 \to \infty$), only limited by mass transfer, the Nernst equation does apply at the electrode surface, leading to concentration overpotentials (assuming the same diffusion coefficients for both species A and B):

$$\begin{aligned} E_{eq} &= E^0_{A/B} + (RT/nF)\text{Ln}[(c_A(0)/c_{Ao})/(c_B(0)/c_{Bo})] \\ &= E_{1/2} + (RT/nF)\text{Ln}[(j - j_{lc})/(j_{la} - j)] \end{aligned}$$

This is the equation of a *polarographic wave*, with $E_{1/2}$ the half-wave potential (Figure 1.4).

Thus,

$$\begin{aligned} \left|\eta_a^{conc}\right| &= \frac{RT}{n_a F}\left|\ln\frac{c_B(0)}{c_{Bo}}\right| = \frac{RT}{n_a F}\left|\ln\left(1 - \frac{|j|}{j_{l_a}}\right)\right| \text{ at the anode} \\ \left|\eta_c^{conc}\right| &= \frac{RT}{n_c F}\left|\ln\frac{c_A(0)}{c_{Ao}}\right| = \frac{RT}{n_c F}\left|\ln\left(1 - \frac{|j|}{j_{l_c}}\right)\right| \text{ at the cathode} \end{aligned} \tag{1.35}$$

where η_i^{conc} is the concentration overpotential (mass transfer limitation). For $|j| \ll j_{li}$ these equations lead to $\eta_i^{conc} \approx R_d\, j$ with $R_d = RT/(n_i F j_{li})$ *the diffusion resistance.*

1.3.3 Cell Voltage versus Current Density Curves

The electrical characteristics E_{cell} (j) can then be obtained by taking into account the different overpotentials (charge transfer overpotentials, mass transfer overpotentials, etc.) and the ohmic losses due to R_e.

For the unit cell, the voltage of the cell E_{cell} (j) is the difference between the positive electrode potential $E^{+}(j)$ and the negative electrode potential $E^{-}(j)$:

$$E_{\text{cell}}(j) = E_c^{+}(j) - E_a^{-}(j) - R_e j = E_{\text{cell}}^{\text{rev}}(j=0) - (|\eta_a| + |\eta_c| + R_e|j|) \tag{1.36}$$

where $E_{\text{cell}}^{\text{rev}}(j=0)$ is the cell voltage under the reversible conditions $(j=0)$ at temperature T and pressure p, R_e is the specific resistance of the cell (electrolyte + interfacial resistance), and η_a and η_c are, respectively, the charge transfer and concentration overpotentials ($\eta_a > 0$ for anodic reactions and $\eta_c < 0$ for cathodic reactions).

E_{cell} versus j characteristics of the fuel cell, taking into account charge transfer overpotentials, concentration overpotentials, and ohmic drop, can thus be written as follows:

$$E_{\text{cell}}(j) = E_c^{+}(j) - E_a^{-}(j) - R_e|j| = E_{\text{eq}} - (|\eta_a^{\text{act}}(j)| + |\eta_a^{\text{conc}}(j)| + |\eta_c^{\text{act}}(j)| + |\eta_c^{\text{conc}}(j)|) - R_e|j|$$

By replacing each contribution of charge transfer and concentration overpotentials by their expressions, one obtains

$$E_{\text{cell}}(j) = E_{\text{cell}}^{\text{rev}} - \frac{RT}{\alpha nF}\ln\left\{\frac{j^2}{j_{o_a} \times |j_{o_c}|}\right\} - \frac{RT}{nF}\left|\ln\left\{\left(1 - \frac{|j|}{j_{l_c}}\right) / \left(1 - \frac{|j|}{j_{l_a}}\right)\right\}\right| - R_e|j| \tag{1.37}$$

Using this last equation, the different contributions to energy losses are illustrated in Figure 1.5 for different j_0 in A cm^{-2} (charge transfer overpotential), cell resistance R_e in Ω cm^{-2} (ohmic losses), and j_l in A cm^{-2} (mass transfer

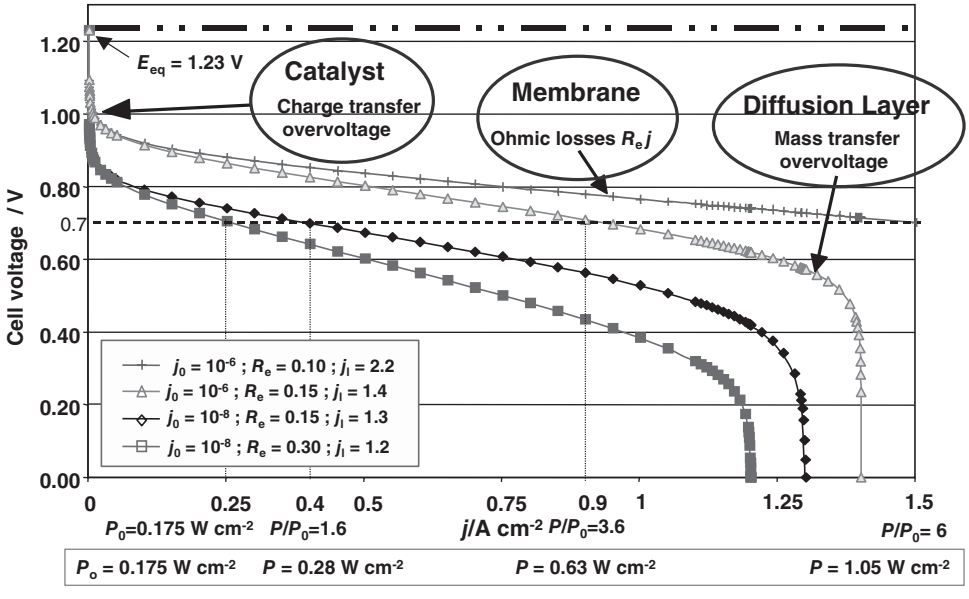

Figure 1.5 Theoretical cell voltage versus current density $E_{\text{cell}}(j)$ curves for a PEMFC: influence of the catalytic properties of electrodes (effect of j_0 on the charge transfer overvoltage), of the membrane specific resistance (effect of R_e on the ohmic losses), and of the mass transfer of reactants (effect of j_l on the mass transfer overvoltage).

overpotential). The effect of each energy loss on j at a given E_{cell} of 0.7 V, that is, on the power density (P) of the cell, is shown for each curve, increasing from $P_0 = 0.175\ W\ cm^{-2}$ for the worse parameters of the membrane–electrode assembly (MEA) to $P = 1.05\ W\ cm^{-2}$ under optimized conditions leading to a sixfold increase in the electric performance of the cell.

1.3.4 Energy Efficiency under Working Conditions ($j \neq 0$)

1.3.4.1 Hydrogen/oxygen Fuel Cell

The electrical energy efficiency of a fuel cell system under working conditions ($j \neq 0$) at temperature T can be defined as the ratio of the electrical energy produced ($W_e = n_{exp} F E_{cell} = -\Delta G_T$) to the total energy used, that is, the chemical energy of combustion ($-\Delta H_T \approx -\Delta H^0$ since $|\Delta H|$ does not vary very much with temperature for H_2O in the gaseous state – see Table 1.1):

$$\varepsilon_{cell} = |\Delta G_T| / (|\Delta H_T| \approx \Delta G_T / \Delta H^0$$

The overall energy efficiency of the fuel cell (ε_{cell}) thus becomes

$$\varepsilon_{cell} = \frac{W_e}{(-\Delta H^0)} = \frac{n_{exp} \times F \times E_{cell}(j)}{(-\Delta H^0)} = \frac{n_{th} F E^0_{eq}}{(-\Delta H^0)} \times \frac{E_{cell}(j)}{E^0_{eq}} \times \frac{n_{exp}}{n_{th}} = \varepsilon_r^{cell} \times \varepsilon_E \times \varepsilon_F \tag{1.38}$$

where $\varepsilon_E = E_{cell}(j)/E^0_{eq}$ is the voltage efficiency referred to standard conditions and $\varepsilon_F = n_{exp}/n_{th}$ is the Faradaic efficiency, that is, the ratio between the number of electrons n_{exp} effectively exchanged in the overall reaction and the theoretical number of electrons n_{th} exchanged for a complete oxidation of the fuel (leading to H_2O for hydrogen and to $H_2O + CO_2$ for a carbonaceous fuel). $\varepsilon_F \approx 1$ for H_2 oxidation but $\varepsilon_F = 4/6 = 0.67$ for the oxidation of CH_3OH stopping at the formation of formic acid (four exchanged electrons instead of six electrons for complete oxidation to CO_2 – see [20]). ε_F depends also on the fuel utilization (stoichiometric ratio).

For the PEM H_2/O_2 fuel cell, the working E_{cell} at 25 °C is typically 0.72 V at $1\ A\ cm^{-2}$ [21], which leads to

$$\varepsilon_E = \frac{E_{cell}(j)}{E^{rev}_{cell}(j=0)} = 1 - \frac{(|\eta_a(j)| + |\eta_c(j)| + R_e\,|j|)}{E^0_{eq}} = \frac{0.72}{1.229} = 0.586 \approx 59\%$$

The overall energy efficiency of a H_2/O_2 fuel cell working at 25 °C and 0.72 V with $j = 1\ A\ cm^{-2}$ is then (see Table 1.1)

$$\varepsilon_{cell}^{H_2/O_2} = \varepsilon_{cell}^{rev} \times \varepsilon_E \times \varepsilon_F = 0.829 \times 0.586 \times 1 = 0.486 \approx 49\ \% \text{ with the HHV}$$

or

$$\varepsilon_{cell}^{H_2/O_2} = \varepsilon_{cell}^{rev} \times \varepsilon_E \times \varepsilon_F = 0.945 \times 0.586 \times 1 = 0.554 \approx 55\ \% \text{ with the LHV.}$$

1.3.4.2 Direct Ethanol Fuel Cell

The overall combustion reaction of C_2H_5OH into O_2 (see reaction (1.21)) corresponds to the following thermodynamic data, under standard conditions

(see Table 1.2):

$$\Delta G^0 = -1326\,\text{kJ mol}^{-1};\ \Delta H^0 = -1367\,\text{kJ mol}^{-1}\ \text{of}\ C_2H_5OH.$$

This gives a standard electromotive force (e.m.f.) at equilibrium:

$$E^{o}_{eq} = -\frac{\Delta G^0}{nF} = \frac{1326 \times 10^3}{12 \times 96485} = E^0_2 - E^0_1 = 1.145\,\text{V}$$

with $n = 12$ the number of electrons exchanged per molecule for complete oxidation to CO_2 – see reaction (1.19). The corresponding electrical energy, $W_{el} = nF\,E^0_{eq} = -\Delta G^0$, leads to a mass energy density $W_e = -\Delta G^0/(3600\,M) = 8.00$ kWh kg^{-1}, where $M = 0.046$ kg is the molecular weight of C_2H_5OH.

The theoretical energy efficiency of a direct ethanol fuel cell (DEFC), under reversible standard conditions, defined as the ratio between the electrical energy produced ($-\Delta G^0$) and the heat of combustion ($-\Delta H^0$) at constant pressure, is (see Eq. (1.8)) as follows:

$$\varepsilon^{rev}_{cell} = \frac{\Delta G^0}{\Delta H^0} = \frac{1326}{1367} = 0.969 \approx 97\%$$

But under working conditions, at a given j, $E_{cell}(j)$ is lower than E^0_{eq} (see Eq. (1.24)), so the practical energy efficiency, for a DEFC working at 0.5 V and 100 mA cm^{-2} with complete oxidation to CO_2, would be (see Eq. (1.38)) as follows:

$$\varepsilon^{C_2H_5OH/O_2}_{cell} = \varepsilon^{rev}_{cell} \times \varepsilon_E \times \varepsilon_F = 0.969 \times 0.437 \times 1 = 0.423 \approx 42\%$$

since $\varepsilon_E = (E_{cell}(j)/E^0_{eq}) = (0.5/1.145) = 0.437$ and $\varepsilon_F = (n_{exp}/n_{th}) = 1$ for complete oxidation to CO_2. This is quite similar to that of the best thermal engine (diesel engine). However, if the reaction process stops at the acetic acid stage, which involves the transfer of 4 electrons (instead of 12 for complete oxidation), the efficiency will be reduced by two-thirds, reaching only 14%.

An additional problem arises from C_2H_5OH crossover through the PEM. It results that the platinum (Pt) cathode experiences a mixed potential, since both the ORR and the C_2H_5OH oxidation take place at the same electrode. The cathode potential is thus lower, leading to a further decrease in E_{cell} and a decrease in ε_E.

1.4 Influence of the Properties of the PEMFC Components (Electrode Catalyst Structure, Membrane Resistance, and Mass Transfer Limitations) on the Polarization Curves

In the $E(j)$ characteristics given in Figure 1.5, one may distinguish three zones associated with the main energy losses encountered in a PEMFC, each corresponding to the influence of the characteristics of the components of the MEA: catalytic properties of the electrodes, specific resistance of the membrane, and mass transfer in the electrode structure [21]. Thus, these three key points will determine the energy efficiency and the specific power of the elementary fuel cell: in these theoretical examples, an improvement in each component of the cell will increase the power density from 0.175 to 1.05 W cm^{-2}, that is, an increase by a

factor of 6. As a consequence for the fuel cell systems, the weight and volume will be decreased by a similar factor, for a given power of the system, and presumably the overall cost will be similarly diminished. The improvement in the components of the elementary fuel cell has a direct effect on the system technology and therefore on the overall cost.

1.4.1 Influence of the Catalytic Properties of Electrodes

The effect of the nature of the catalytic layer is particularly visible at the beginning of the $E(j)$ characteristics (low current densities) and corresponds to the charge transfer polarization, that is, the activation overpotentials due to a relatively low electron transfer rate at the electrode–electrolyte interface. This comes mainly from the ORR whose j_0 is much smaller than that of the HOR. An increase in j_0 from 10^{-8} to 10^{-6} A cm^{-2} leads to an increase in j (at 0.7 V) from 0.4 to 0.9 A cm^{-2}, that is, an increase in the energy efficiency and in the power density by 3.6 times compared to the initial curve (Figure 1.6).

Similar behavior is encountered in the electrooxidation of alcohols, whose kinetics is rather slow, which needs active catalysts to increase j_0 and thus j at a given E_{cell}, as shown in Figure 1.7 for a DEFC [8].

1.4.2 Influence of the Membrane-specific Resistance

The E versus j linear part of the $E(j)$ characteristics corresponds to ohmic losses $R_e \mid j \mid$ resulting from R_e due to the electrolyte and interface resistances. A decrease

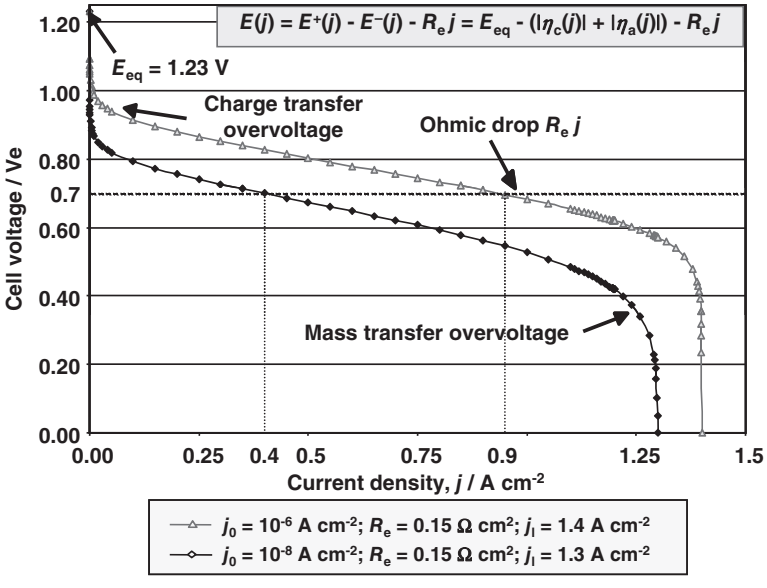

Figure 1.6 Influence of the catalytic properties of electrodes ($j_0 = 10^{-8}$ or 10^{-6} A cm^{-2}) on the E_{cell} versus j characteristics $E(j)$. *Source:* Lamy 2011 [21]. Reproduced with permission of Elsevier.

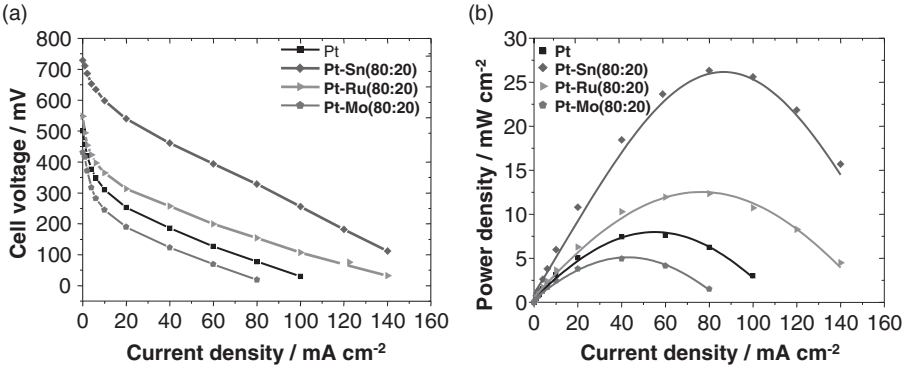

Figure 1.7 Fuel cell characteristics of a DEFC recorded at 110 °C: (a) polarization curves; (b) power density curves. Influence of the nature of the Pt-based catalyst (30% loading loading on XC72 carbon powder) containing tin (Sn), ruthenium (Ru), or molybdebum (Mo). Anode catalyst: 1.5 mg cm^{-2}; cathode catalyst: 2 mg cm^{-2} (40% Pt/XC72 E-TEK); membrane: Nafion® 117; C_2H_5OH concentration: 1 M. (Reproduced with permission from Ref. [8]. Copyright 2009 Wiley-VCH.)

in the specific electric resistance R_e from 0.3 to 0.15 Ω cm^2 leads to an increase in j (at 0.7 V) from 0.25 to 0.4 A cm^{-2}, that is, an increase in the energy efficiency and in the power density by 1.6 times (see Figure 1.5). This was experimentally observed by Ballard Power Systems when comparing the behavior of Nafion® and Dow® membranes, which are sulfonated perfluorinated membranes (Figure 1.8) [22].

1.4.3 Influence of the Mass Transfer Limitations

The effect of the structure of the gas diffusion layer (GDL) controls j_l associated with mass transfer limitations for the reactive species and reaction products to and/or from the electrode active sites. An increase in j_l from 1.4 to 2.2 A cm^{-2} leads to a further increase in j (at 0.7 V) from 0.9 to 1.5 A cm^{-2}, that is, an increase

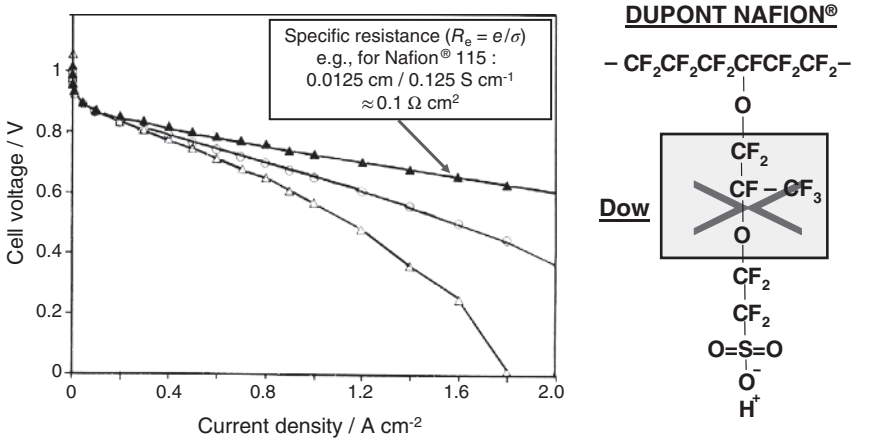

Figure 1.8 *E*(*j*) characteristics of an elementary PEMFC with different membranes: ▲ Dow ($e = 125$ μm); o Nafion® 115 ($e = 125$ μm); △ Nafion® 117 ($e = 175$ μm).

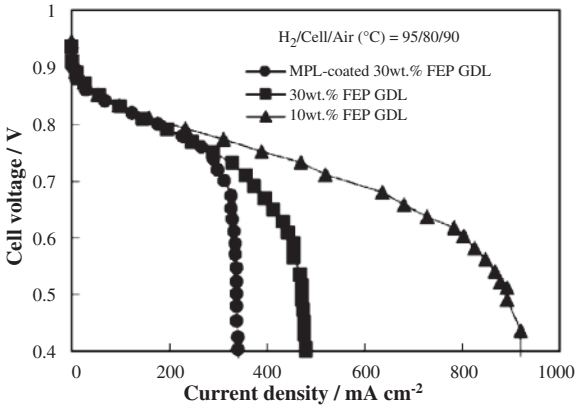

Figure 1.9 E_{cell} versus j curves for a H_2/air fuel cell with MEAs using three different types of carbon cathode GDLs (80 °C, 0.22 mg cm^{-2} Pt loading): (●) MPL-coated with 30 wt.% FEP impregnated; (■) 30 wt.% FEP impregnated; (▲) 10 wt.% FEP impregnated. *Source:* Lim 2004 [23]. Reproduced with permission of Elsevier.

in the energy efficiency and in the power density by six times compared to the initial curve with $j_0 = 10^{-8}$ A cm^{-2}, $R_e = 0.30\ \Omega$ cm^2 and $j_l = 1.2$ A cm^{-2} (Figure 1.5). This was experimentally observed for three different GDLs of different composition at the air cathode: a microporous layer (MPL), coated with 30 wt.% fluorinated ethylene propylene (FEP), and two other FEP-impregnated layers with 30 and 10 wt.% FEP, respectively (Figure 1.9) [23].

1.5 Representative Examples of Low-temperature Fuel Cells

Several review papers on fuel cells and their different applications have been recently published. For example, Sharaf and Orhan presented many possible applications of the different kinds of fuel cells, particularly for portable electronics and the electric vehicle [24], whereas Wang *et al.* focused their paper on PEMFCs, their technology, and applications mainly for the electric vehicle [25]. Li and Faghri did a review of DMFC stacks for recharging Li-ion batteries for portable equipments and on portable fuel cell systems for soldiers [26]. On the other hand, many review papers on PEMFCs for the electrical vehicle can be found in recent publications [27–29].

1.5.1 Direct Methanol Fuel Cell for Portable Electronics

The electrocatalytic oxidation of CH_3OH has gained much interest over a number of years because it is the simplest alcohol which can be completely oxidized to CO_2 in a DMFC [6,7,30], thus providing the maximum energy densities (6.1 kWh kg^{-1} or 4.8 kWh dm^{-3}). The great advantage of a DMFC is that CH_3OH is a liquid fuel, thus more easily handled and stored than H_2. Moreover, CH_3OH is produced in large quantities from natural gas by steam methane reforming (SMR) at a low cost (~0.2 US dollar per liter), making it a key product in the chemical industry. Its toxicity is relatively low and its boiling point (~65 °C) makes it liquid for most

utilization. The development of PEM led to great simplification of DMFC by avoiding a fuel processor that must provide a reformate gas with a low concentration of carbon monoxide (CO) (<10 ppm, otherwise it may strongly poison the catalysts used in the Pt-based anode). Due to system simplicity, DMFCs are particularly efficient power sources for portable electronics (cell phones, laptop computers, cam recorders, etc.) and for small-size applications (micropower sources, power sources for the soldier, propulsion of small devices such as golf carts, drones, etc.).

A DMFC consists of two electrodes, a catalytic CH_3OH anode, and a catalytic O_2 cathode, separated by an ionic conductor, preferably an acid electrolyte, for rejecting the CO_2 produced. Great progress was made by feeding CH_3OH directly to the anodic compartment of a PEMFC, in which the protonic membrane, for example, Nafion®, plays the role both of an acidic medium and of a separator between the two electrode compartments (Figure 1.10). This technology has the added advantage of thin elementary cells and hence of compact stacks.

The electrochemical oxidation of CH_3OH occurs on the anode electrocatalyst (e.g., dispersed Pt-based catalysts), which constitutes the negative pole of the cell:

$$CH_3OH + H_2O \rightarrow CO_2 + 6\,H^+ + 6\,e^- \quad \text{in acid electrolytes} \tag{1.18}$$

$$CH_3OH + 8\,OH^- \rightarrow CO_3^{2-} + 6\,H_2O + 6\,e^- \quad \text{in alkaline electrolytes} \tag{1.39}$$

whereas the electrochemical reduction of O_2 occurs at the cathode (also containing a Pt-based catalyst) that constitutes the positive pole of the cell:

$$1/2\,O_2 + 2\,H^+ + 2\,e^- \rightarrow H_2O \quad \text{in acid electrolytes} \tag{1.13}$$

$$1/2\,O_2 + H_2O + 2\,e^- \rightarrow 2\,OH^- \quad \text{in alkaline electrolytes} \tag{1.40}$$

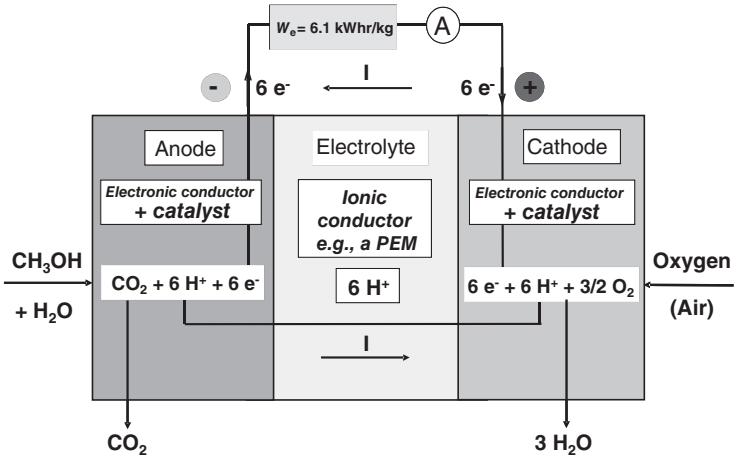

Figure 1.10 Schematic diagram of a DMFC based on a PEM. *Source:* Lamy 2014 [20]. Reproduced with permission of Springer.

The overall reaction corresponds thus to the catalytic combustion of CH_3OH into O_2:

$$CH_3OH + 3/2\,O_2 \rightarrow CO_2 + 2\,H_2O \qquad \text{in acid electrolytes} \tag{1.20}$$

$$CH_3OH + 3/2\,O_2 + 2\,OH^- \rightarrow CO_3^{2-} + 3\,H_2O \qquad \text{in alkaline electrolytes} \tag{1.41}$$

One main advantage of such a power source is the direct transformation of the chemical energy of CH_3OH combustion into electrical energy, thus avoiding a low energy efficiency given by the Carnot's theorem for thermal engines. Hence, E_{cell}^{rev} can be calculated from the Gibbs energy change, ΔG_r, associated with the total combustion reaction of CH_3OH (reaction (1.20)), by the following equation:

$$\Delta G_r + nFE_{cell}^{rev} = 0 \quad \text{leading to} \quad E_{cell}^{rev} > 0$$
$$\text{since } \Delta G_r < 0 \text{ (spontaneous reaction)}$$

where $n = 6$ is the number of Faradays (per mole of CH_3OH) involved in the half-cell reaction (1.18) or (1.39).

Under standard conditions (25 °C), the enthalpy change ΔH^0 for reaction (1.20), is $-726\,kJ\,mol^{-1}$ of CH_3OH, and the Gibbs energy change ΔG^0 is $-702\,kJ\,mol^{-1}$ of CH_3OH (see Table 1.2). This corresponds to a standard reversible cell voltage (E_{cell}^0) as given by the following equation:

$$E_{cell}^0 = E_c^0 - E_a^0 = -\frac{\Delta G^0}{nF} = \frac{702 \times 10^3}{6 \times 96485} = 1.213\,V$$

where E_c^0, E_a^0, the standard potentials of each electrode versus SHE used as a reference electrode, are defined as the difference of the inner potential at each electrode–electrolyte interface.

The main features of the DMFC are its high specific energy (W_s) and high volume energy density (W_{sl}), the values of which are calculated as follows:

$$W_s = \frac{(-\Delta G^0)}{3600 \times M} = \frac{702 \times 10^3}{3600 \times 0.032} = 6.09\,kWh\,kg^{-1}$$

and $W_{sl} = W_s \times \rho = 4.82\,kWh\,dm^{-3}$, where $M = 0.032\,kg$ is the molar weight of CH_3OH and $\rho = 0.7914\,kg\,dm^{-3}$ its density.

Under standard reversible conditions (25 °C), the energy efficiency is very high:

$$\varepsilon_{cell}^{rev} = \frac{W_e}{(-\Delta H^0)} = \frac{nFE_{cell}^0}{(-\Delta H^0)} = \frac{\Delta G^0}{\Delta H^0} = \frac{702}{726} = 0.967 \approx 97\%$$

It is much higher than that of a H_2/O_2 fuel cell (i.e., 83%) under standard conditions. However, under usual operating conditions, at a given j, the electrode potentials deviate from their equilibrium values due to large overpotentials, η_i, at both electrodes (Figure 1.11):

$$\eta_a = E_a(j) - E_a^0 \geq 0 \qquad \text{at the } CH_3OH \text{ anode}$$

$$\eta_c = E_c(j) - E_c^0 \leq 0 \qquad \text{at the } O_2 \text{ cathode}$$

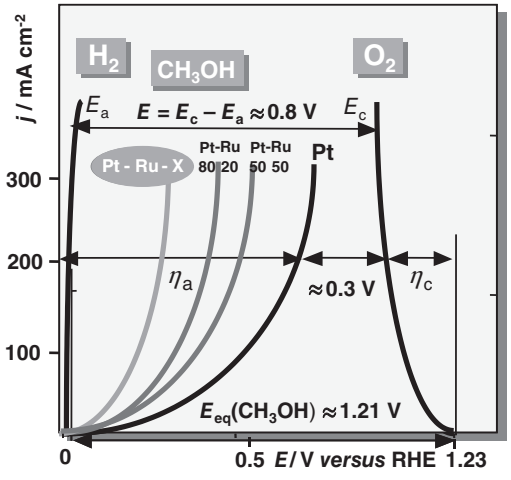

Figure 1.11 *j*(*E*) characteristics for the electrochemical reactions involved in a H_2/O_2 PEMFC and in a DMFC. *Source:* Lamy 2014 [20]. Reproduced with permission of Springer.

This results from a slow kinetics of both CH_3OH oxidation and ORR. An additional loss is due to R_e (arising mainly from the proton conducting membrane). E_{cell} under working conditions is thus

$$E_{cell}(j) = E_c(j) - E_a(j) - R_e\, j = E_{cell}(0) - (|\eta_c| + |\eta_a| + R_e\, j) \leq E_{cell}(0) \qquad (1.36)$$

so the energy efficiency will be decreased proportionally to the voltage efficiency ε_E.

For a DMFC working at 200 mA cm^{-2} and 0.5 V (e.g., with a Pt-Ru anode), this ratio will be

$$\varepsilon_E = 0.5/1.21 = 0.413 = 41.3\%$$

and the overall efficiency of the fuel cell will be (see Eq. (1.38))

$$\varepsilon_{cell}^{MeOH} = \varepsilon_{cell}^{rev} \times \varepsilon_E \times \varepsilon_F = 0.967 \times 0.413 \times 1 = 0.399 \approx 40\%$$

assuming a Faradaic efficiency of 100%, that is, the total oxidation of CH_3OH. This is acceptable for an autonomous power source oxidizing CH_3OH completely to CO_2 and giving the theoretical number of Faradays $n_{th} = 6$ F per mole of CH_3OH – see reaction (1.18) or (1.39). However, under some operating conditions CH_3OH oxidation to CO_2 is not complete, so a Faradaic efficiency is introduced, $\varepsilon_F = n_{exp}/n_{th}$, where n_{exp} is the number of Faraday effectively exchanged in the half-cell reaction.

Therefore, the overall efficiency $\varepsilon_{cell}^{MeOH} = \varepsilon_{cell}^{rev} \times \varepsilon_E \times \varepsilon_F$ may be dramatically decreased, for example, if the electrooxidation stops at the formaldehyde stage:

$$CH_3OH \rightarrow HCHO + 2\,H_{aq}^{+} + 2\,e^{-} \qquad (n_{exp} = 2)$$

or at the formic acid stage:

$$CH_3OH + H_2O \rightarrow HCOOH + 4\,H_{aq}^{+} + 4e^{-} \qquad (n_{exp} = 4)$$

thus leading, respectively, to a Faradaic efficiency:

$$\varepsilon_F = n_{exp}/n_{th} = 2/6 = 0.333$$

or

$$\varepsilon_F = n_{exp}/n_{th} = 4/6 = 0.667$$

and, respectively, to an overall energy efficiency:

$$\varepsilon_{cell}^{MeOH} = \varepsilon_{cell}^{rev} \times \varepsilon_E \times \varepsilon_F = 0.967 \times 0.413 \times 0.333 = 0.133 \approx 13\%$$

or

$$\varepsilon_{cell}^{MeOH} = \varepsilon_{cell}^{rev} \times \varepsilon_E \times \varepsilon_F = 0.967 \times 0.413 \times 0.667 = 0.266 \approx 27\%$$

The electrical characteristic of a DMFC depends strongly on the nature and structure of the anode catalysts. Pt-Ru nanoparticle catalysts dispersed on an electron conductive substrate, such as Vulcan XC-72R carbon powder, give the best results. The bimetallic composition is particularly important and the optimum atomic composition corresponds to 20% Ru versus 80% Pt, that is, an atomic ratio of Pt:Ru close to 4 : 1, as discussed in Section 3.3.4.1 of Chapter 3. This is illustrated in Figure 1.12 [31].

DMFC systems are, therefore, competitive with energy density on the order of 400 Wh kg^{-1} or 500–800 Wh l^{-1}, which is two–three times greater than that of a Li-ion battery [26]. DMFC systems have been developed by several companies all around the world: Toshiba, Sony, Panasonic, Sharp, Hitachi in Japan; Samsung in South Korea; Jet Propulsion Laboratory, MTI Microfuel Cells, Oorja Protonics, Relion in USA; ZSW, Julich Center, Smart Fuel Cells, Baltic Fuel Cells in Germany;

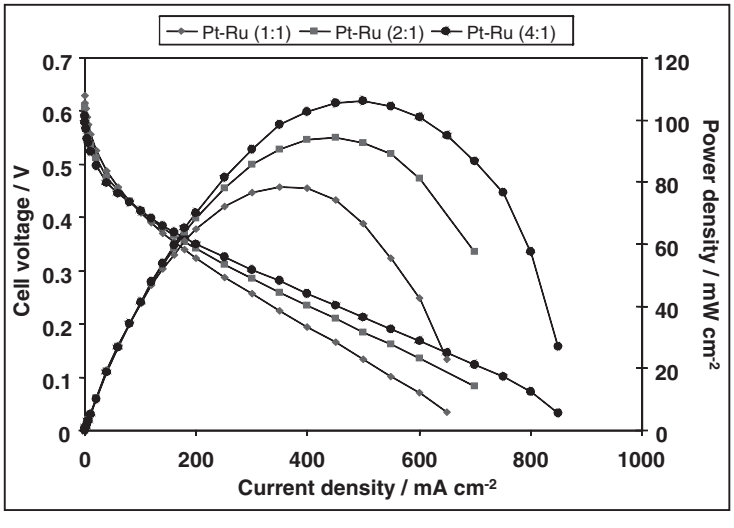

Figure 1.12 *E*(*j*) and *P*(*j*) curves of a single DMFC with Pt-Ru/C electrodes of different Pt-Ru atomic ratios. Anode loading: 2 mg cm^{-2} Pt-Ru/C; membrane: Nafion® 117; cathode loading: 2 mg cm^{-2} Pt/C; [MeOH] = 2 M, 2 ml min^{-1}, p_{MeOH} = 2 bar; T_{cell} = 110 °C; O_2 = 120 ml min^{-1}, p_{O2} = 2.5 bar; $T_{MeOH} = T_{O2}$ = 95 °C. *Source:* Coutanceau 2004 [31]. Reproduced with permission of Springer.

Figure 1.13 TOSHIBA DMFC for portable applications. Direct methanol fuel cell combined with a small backup Li-ion battery. *Source:* Han 2002 [32]. Reproduced with permission of Elsevier.

CMR Fuel Cells Limited in UK; and Cellera Technologies in Israel. They can be used as small power sources, mainly for portable electronics (cell phone, notebook PC, music player, electric tools, soldier equipment, etc.) with liquid CH_3OH stored either in a small cartridge or in a small tank. In most of these technologies, the DMFC provides power for recharging a Li-ion battery, thus extending greatly its autonomy and allowing a quick recharge of the system by refilling the tank with fresh CH_3OH.

This last point is illustrated in Figures 1.13 and 1.14 showing a Toshiba DMFC of 5 W to recharge a Li-ion battery for a cell phone [32] and a LG Chemical DMFC of 25 W to power a laptop computer [26]. Eight unit cells, each having 9 cm^2 of active surface area, are connected in series [32] in order to raise the output voltage to 2.5–3.9 V, which is the typical voltage range for most cell phone applications.
Finally to favor the commercial issue of DMFC, new low-cost components have to be developed, particularly catalysts with a lower amount of platinum group metals (PGMs) or even with no noble metals, and high-temperature-resistant membranes of lower cost than Nafion® and of higher protonic conductivity and stability to operate the DMFC at higher temperatures (150–200 °C), which may increase the power density through thermal activation of the reaction kinetics.

Figure 1.14 The 25 W DMFC prototype to power laptop computers, by LG Chemical in 2005. *Source:* Li 2013 [26]. Reproduced with permission of Elsevier.

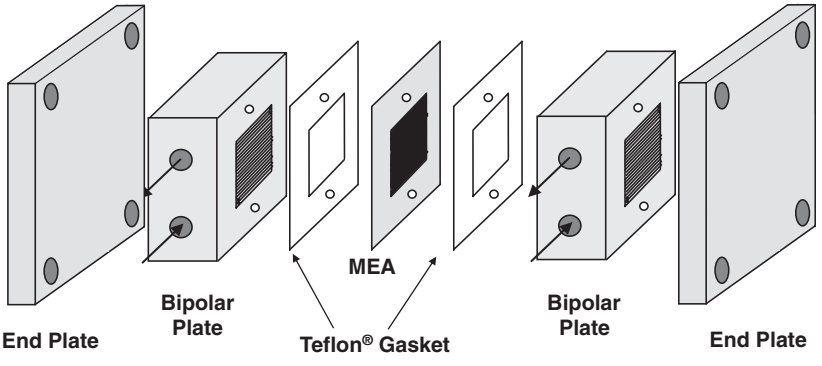

Figure 1.15 Schematic representation of a PEMFC elementary cell. *Source:* Lamy 2011 [21]. Reproduced with permission of Elsevier.

1.5.2 Hydrogen/air PEMFC for the Electrical Vehicle

An elementary PEMFC comprises several elements and components: the MEA, the flow-field plate (bipolar plate (BP), which also ensures electric contact with the next cell and evacuation of excess heat), gaskets to ensure tightness to reactants, and end plates (Figure 1.15).

The MEA consists of a thin (10–200 μm) solid polymer electrolyte (a protonic membrane, such as Nafion®) on both sides of which are pasted the electrode structures (fuel anode and O_2 cathode) (Figure 1.16). The electrode structure comprises several layers: a first layer made of carbon paper (or cloth) to strengthen

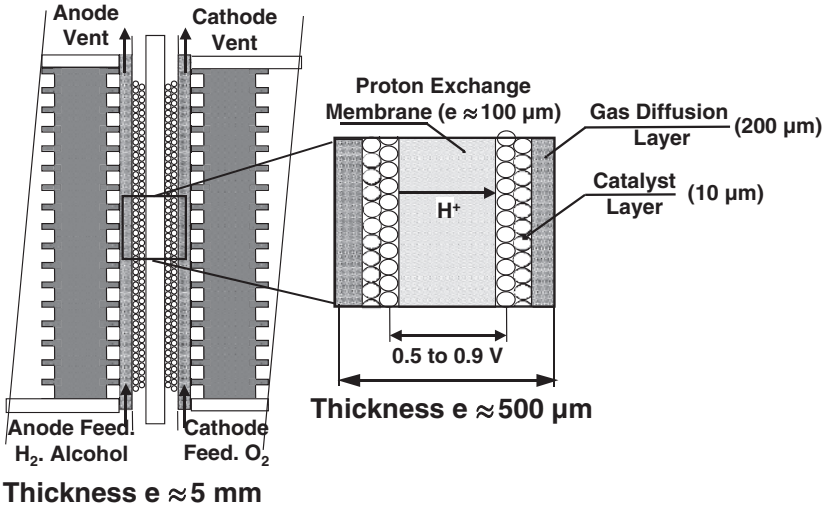

Figure 1.16 Schematic representation of the MEA of a PEMFC. *Source:* Lamy 2011 [21]. Reproduced with permission of Elsevier.

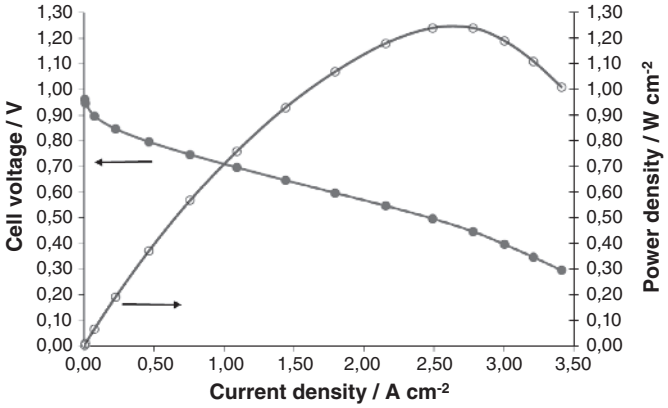

Figure 1.17 Performance of a MEA fabricated with Pt/C catalysts synthesized by the colloidal method. Membrane: Nafion® 112; symmetric electrodes: 0.35 mg_{Pt} cm^{-2}; Pt loading 40 wt.%/C ($T_{cell} = T_{huma} = 70$ °C, $T_{humc} = 25$ °C, H_2 flow = 600 ml min^{-1}, O_2 flow = 300 ml min^{-1}, $p_{H2} = p_{O2} = 3$ bar). (Reproduced with permission from Ref. [21]. Copyright 2011 Elsevier.)

the structure, on which are coated the GDLs, and then the catalyst layer (CL), directly in contact with the protonic membrane [10].

The PEM, which is a solid polymer electrolyte, plays a key role in the PEMFC. It allows the electrical current to pass through it thanks to its H^+ ionic conductivity and prevents any electronic current through it in order that electrons are obliged to circulate in the external electric circuit to produce the electric energy corresponding to the combustion reaction of the fuel; it must avoid any gas leakage between the anodic and the cathodic compartments, so that no chemical combination between H_2 and O_2 is directly allowed; it must be stable mechanically, thermally (up to 150 °C in order to increase the working temperature of the cell) and chemically; and finally, its lifetime must be sufficient for practical applications (e.g., >2000 h for transportation power trains or >40 000 h for stationary power plant).

Using a Nafion® 212 membrane (50 μm thickness) and optimized Pt/C electrodes, one obtains good electrical characteristics with power density greater than 1.2 W cm^{-2} [21] (Figure 1.17).

A single cell delivers a cell voltage between 0.5 and 0.9 V (instead of $E^0_{eq} = 1.23$ V under standard equilibrium conditions), depending on the working conditions and j, so many elementary cells, electrically connected by the bipolar plates, are assembled together in a filter press configuration (in series and/or in parallel) to reach the nominal voltage (such as 48 V for electric vehicles) and the power needed for a given application. Such fuel cell stacks are able to power an electric vehicle, for example, the FCveloCity® fuel cell stacks (developed by Ballard Power Systems) that can deliver electric power from 4 to 21 kW [33] (Figure 1.18).

The actually developed PEMFC have a Nafion® membrane, which partially fulfills these requirements, since its thermal stability is limited to 100 °C and its protonic conductivity strongly decreases at higher temperatures because of its dehydration. On the other hand, it is not completely tight to liquid fuels (such as alcohols). This is as important as the membrane is thin (a few 10 μm). Furthermore,

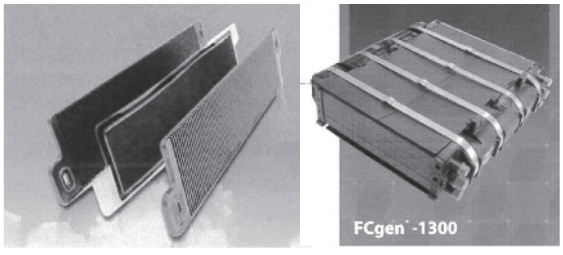

Figure 1.18 New generation of Ballard fuel cell stacks such as FCgen-1300 (2.4–10 kW). *Source:* Lamy 2011 [21]. Reproduced with permission of Elsevier.

its actual cost is still too high (about € 400 per m^2), so its use in a PEMFC for a low-cost passenger electric car is still a challenge.

One of the main problems of low temperatures (20–90 °C) PEMFCs is the relatively low kinetics rate of the electrochemical reactions involved, for example, ORR at the cathode and fuel (pure H_2 or H_2 from a reformate gas) oxidation at the anode. Pt-based catalysts are actually the only efficient catalysts used in commercial PEMFCs, but PGM loading of the electrode is still too high, particularly at the O_2 electrode, leading to a large part of the MEA cost. Another problem, particularly crucial for the electric vehicle, is the relatively low working temperature (70–90 °C), which prevents efficient exhaust of the excess heat generated by the power fuel cell. Therefore, new membranes, such as polybenzimidazole [34], are investigated with improved stability and conductivity at higher temperatures (up to 150 °C). For power fuel cells, the increase in temperature will increase the rate of the electrochemical reactions occurring at both electrodes, that is, j at a given E_{cell} and the specific power. Furthermore, thermal management and heat utilization will be improved, particularly for residential applications with heat cogeneration, and for large-scale applications to exhaust excess heat.

Fuel supply is usually from liquid H_2 or pressurized gaseous H_2 (between 350 and 700 bars). For other fuels, such as natural gas, CH_3OH, and so on, a fuel processor is needed, which includes a reformer, water gas shift reactors, and purification reactors (in order to decrease – a few tens of parts per million – the amount of CO to an acceptable level, which would otherwise poison the Pt-based catalysts). This equipment is still heavy and bulky and limits the dynamic response of the fuel cell stack, particularly for the electric vehicle in some urban driving cycle. In addition, the nature of other auxiliary equipment depends greatly on the stack characteristics and targeted applications (Figure 1.19):

- Air compressor, the characteristics of which are related to the differential pressure supported by the PEM
- Humidifiers for the reacting gases with controlled humidification conditions
- Preheating of gases to avoid any condensation phenomena
- H_2 recirculation, purging system of the anode compartment
- Cooling system for MEAs
- Control valves of pressure and/or gas flows
- DC/DC or DC/AC electric converters

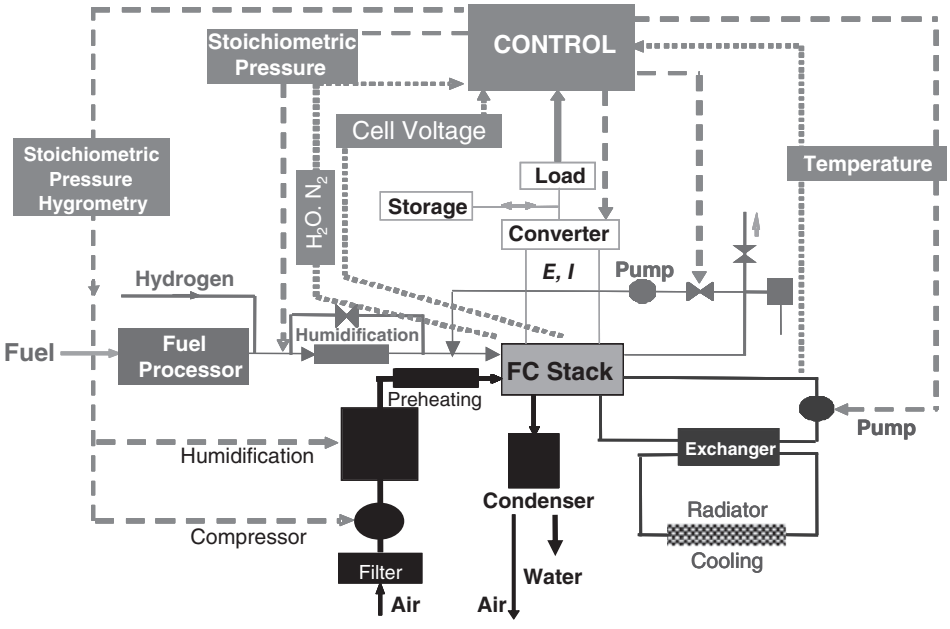

Figure 1.19 Detailed scheme of a PEMFC system with its auxiliary and control equipment. (Reproduced with permission from Ref. [21]. Copyright 2011 Elsevier.)

The system control must ensure correct working of the system, not only under steady-state conditions but also during power transients. All the elementary cells must be controlled (measurement of E_{cell} of each elementary cell, if possible) and the purging system must be activated in case of technical incident.

The electrical energy efficiency of such a device is very high, reaching 55% under usual operating conditions ($T = 70\,°C$, $p = 2$ to 3 bars). This is at least two–three times more than the energy efficiency of an ICE, so the PEMFC stacks are very attractive sources for the electric vehicle [24]. Moreover, the thickness of an elementary cell is rather small (on the order of a few millimeters), so PEMFC stacks of 10–100 kW, consisting of a few hundred elementary cells in series (Figure 1.20), are very compact leading to high power density (3.1 kW kg^{-1} or 2.5 kW dm^{-3} for the stack) and about 1 kW per kg or per liter for the entire system (fuel cell stack with its auxiliary components), fitting easily under the hood of the car.

Therefore, PEMFCs provide power trains to car manufacturers for their electrical vehicles with near-zero harmful emissions without having to compromise the efficiency of the vehicle's propulsion system. Due to their inherent advantages, such as static operation, fuel flexibility, modularity, dynamic response, low operation temperatures, and low maintenance requirements, fuel cells become an ideal alternative to the actual ICEs, provided that durability, low cost, H_2 infrastructure, and technical targets are met on schedule. Japan, for example, plans to deploy 2 million fuel cell electric vehicles (FCEVs) with 1000 hydrogen refueling stations by 2025 [24]. Many car manufacturers (General Motors, Toyota, Mazda, Daimler AG, Volvo, Volkswagen, Honda, Hyundai, Nissan, etc.) have

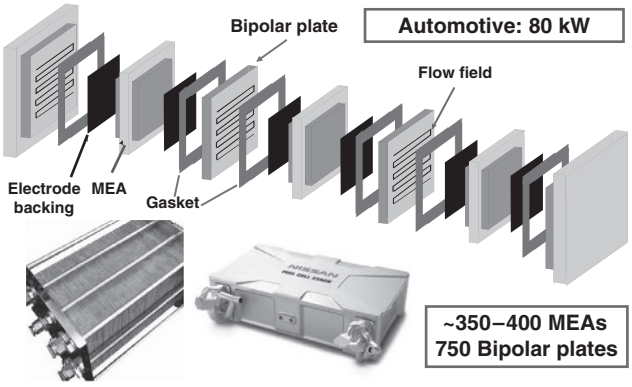

Figure 1.20 Fuel cell stack of 80 kW for transportation applications.

demonstrated the feasibility of electrical vehicles equipped with a fuel cell stack to power the main propulsion system (Figure 1.21). Some of them have begun the commercialization of FCEVs, such as the ix35 [35] of Hyundai (Korea) at the beginning of 2013 in Denmark and Sweden, and the Toyota Mirai at the end of 2015 in Japan and California.

As an example, the Toyota Mirai (Figure 1.22) is a five-seat compact car equipped with a 114 kW PEMFC stack (volumetric specific power of 3.1 kW dm^{-3}), allowing a maximum speed of 175 kmph, a nickel metal hydride battery and two fuel tanks with a total of 122 l of compressed H_2 at 700 bars (weight storage density of 5.7%) providing an autonomy close to 600 km [36].

In Europe, Daimler AG is ready to commercialize its B-Class with a fuel cell stack of 100 kW and a Li-ion battery of 1.4 kWh leading to a maximum speed of

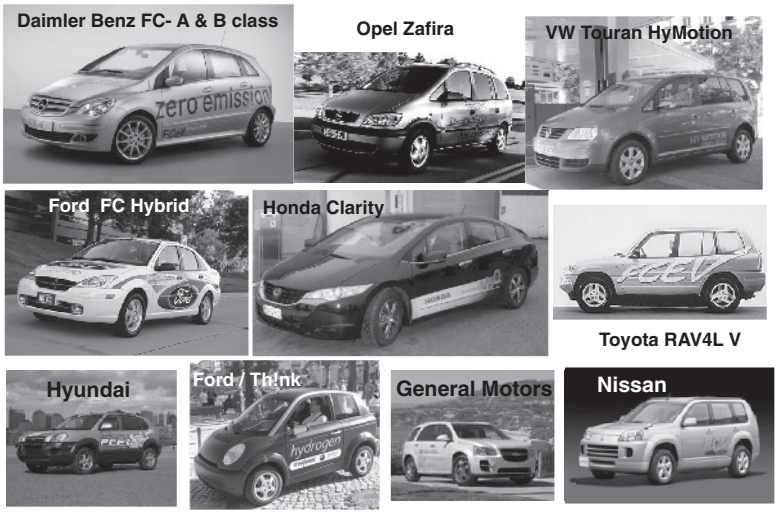

Figure 1.21 Some examples of FCEVs ready to be commercialized.

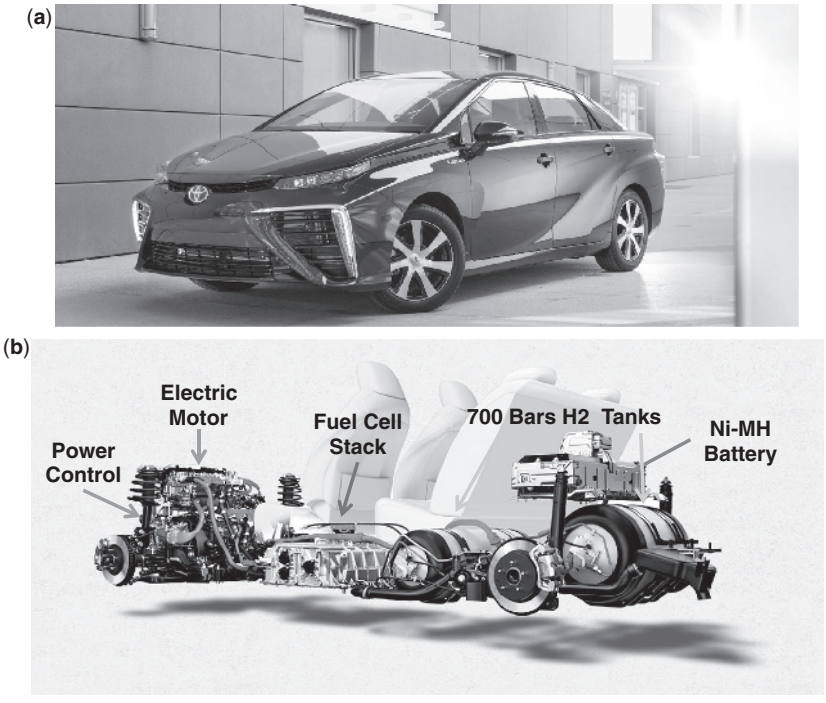

Figure 1.22 View of the Toyota Mirai (a) with the implantation architecture of its different elements (b).

170 kmph and autonomy of about 400 km with a H_2 tank of 3.7 kg at 700 bars (Figure 1.23) [37].

1.6 Conclusions and Outlook

The actual development of LT PEMFCs fed either with H_2 or with a liquid fuel, such as an alcohol (CH_3OH, C_2H_5OH, etc.), gives us new opportunities to improve our environment, by providing electric power sources with good energy efficiency (40–55%) and near zero emissions of pollutants (except for the production of H_2 from carbon-containing fossil fuel, for example, by SMR).

The H_2/O_2 (air) PEMFC is nearly mature to power the electric vehicle and automakers are quite ready to commercialize such cars, provided hydrogen refueling stations are put in place everywhere. This is the responsibility of federal and local governments, for example, California in the United States, to promulgate the corresponding laws in order to improve the air quality of large cities (e.g., Los Angeles) by preventing any emissions of deleterious gases (NO_x, SO_x, etc.) or GHGs (i.e., CO_2) produced by ICE cars still consuming fossil fuels.

On the other hand, small DAFCs, particularly the DMFCs, are developing rapidly for powering portable electronics, either to recharge their lithium battery

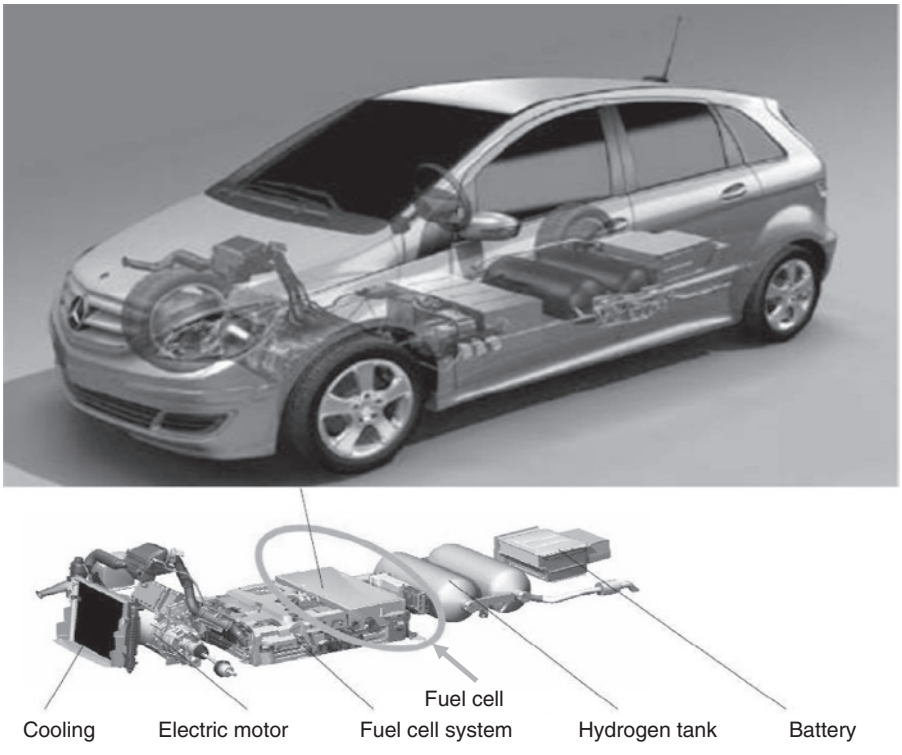

Figure 1.23 Fuel cell stack module and power train of the Daimler B-Class fuel cell car.

or to supply power directly to them, due to their ease of fuel refueling and greater autonomy compared to the lithium batteries.

Further progress in the development of LT PEMFCs, either the H_2/O_2 PEMFC or the DAFC (DMFC or DEFC), depends on the investigation of improved or new electrocatalysts, particularly for the ORR and the AOR, which is still a challenge for scientists and engineers working in the field of electrocatalysis.

Acknowledgments

Part of this chapter was presented at the International Summer School on "PEM Fuel Cells" organized in June 2013 at Bursa (Turkey) by the European Commission, Directorate General Joint Research Centre (JRC), Institute for Energy and Transport (IET). I would like to thank particularly Dr. G. Tsotridis for his kind invitation to participate as a lecturer.

References

1 Stolten, D. (2010) *Hydrogen and Fuel Cells, Fundamentals, Technologies and Applications*, Wiley-VCH Verlag Gmbh, Weinheim.

2 Sørensen, B. (2005) *Hydrogen and Fuel Cell Emerging Technologies and Applications*, Elsevier Academic Press, New York.
3 Barbir, F. (2005) *PEM Fuel Cells: Theory and Practice*, Elsevier Academic Press, New York.
4 Carrette, L., Friedrich, K.A., and Stimming, U. (2000) Fuel cells: principles, types, fuels, and applications. *ChemPhysChem*, **1**, 162–193.
5 Lamy, C. (2006) Operation of fuel cells with biomass resources (hydrogen and alcohols), in *Waste Gas Treatment for Resource Recovery* (eds P. Lens, C. Kennes, P.L. Cloirec, and M. Deshusses), IWA Publishing, London, Chapter 21, pp. 360–384.
6 Lamy, C., Léger, J.-M., and Srinivasan, S. (2001) Direct methanol fuel cells: from a twentieth century electrochemist's dream to a twenty-first century emerging technology, in *Modern Aspects of Electrochemistry*, vol. 34 (eds J.O'M. Bockris, B.E. Conway, and R.E. White), Kluwer Academic/Plenum Publishers, New York, Chapter 3, pp. 53–118.
7 Arico, A., Baglio, V., and Antonucci, V. (2009) Direct methanol fuel cells: history, status and perspectives, in *Electrocatalysis of Direct Methanol Fuel Cells* (eds J.J. Zhang and H. Liu), Wiley-VCH Verlag Gmbh, Weinheim, Chapter 17, pp. 1–78.
8 Lamy, C., Coutanceau, C., and Léger, J.-M. (2009) The direct ethanol fuel cell: a challenge to convert bioethanol cleanly into electric energy, in *Catalysis for Sustainable Energy Production* (eds P. Barbaro and C. Bianchini), Wiley-VCH Verlag Gmbh, Weinheim, Chapter 1, pp. 3–46.
9 Bockris, J.O'.M. and Srinivasan, S. (1969) *Fuel Cells: Their Electrochemistry*, McGraw Hill Book Co., New York.
10 Hoogers, G. (ed.) (2003) *Fuel Cell Technology Handbook*, CRC Press, Taylor & Francis Group, LLC, Boca Raton, Florida.
11 Vielstich, W., Gasteiger, H., and Lamm, A. (2003) *Handbook of Fuel Cells: Fundamentals and Survey of Systems*, vol. 1, John Wiley & Sons, Ltd, Chichester.
12 Lamy, C., Belgsir, E.M., and Léger, J.-M. (2001) Electrocatalytic oxidation of aliphatic alcohols: application to the direct alcohol fuel cells. *J. Appl. Electrochem.*, **31**, 799–809.
13 Lamy, C., Lima, A., Le Rhun, V., Delime, F., Coutanceau, C., and Léger, J.-M. (2002) Recent advances in the development of direct alcohol fuel cells. *J. Power Sources*, **105**, 283–296.
14 Bockris, J.O'M. and Reddy, A.K.N. (1972) *Modern Electrochemistry*, Plenum Press, New York, vol. 2, p. 1141.
15 Sakellaropoulos, G.P. (1981) *Advances in Catalysis* (eds D.D. Eley, H. Pines, and P.B. Weisz), Academic Press, New York, p. 218.
16 Appleby, A.J. (1983) *Comprehensive Treatise of Electrochemistry*, vol. 7 (eds B.E. Conway, J.O'M. Bockris, E. Yeager, S.U.M. Khan, and R.E. White), Plenum Press, New York, pp. 173–239.
17 Rousseau, S., Coutanceau, C., Lamy, C., and Léger, J.-M. (2006) Direct ethanol fuel cell: electrical performances and reaction product distribution under operating conditions with different platinum-based anodes. *J. Power Sources*, **158**, 18–24.
18 Vetter, K.J. (1967) *Electrochemical Kinetics, Theoretical and Experimental Aspects*, Academic Press, New York.

19 Bard, A.J. and Faulkner, L.R. (1980) *Electrochemical Methods: Fundamentals and Applications*, John Wiley & Sons, Inc, New York.
20 Lamy, C. (2014) Anodic reactions in electrocatalysis: methanol oxidation, in *Encyclopedia of Applied Electrochemistry* (eds G. Kreysa, K.I. Ota, and R.F. Savinell), Springer, Online, pp. 85–92.
21 Lamy, C., Jones, D., Coutanceau, C., Brault, P., Martemianov, S., and Bultel, Y. (2011) Do not forget the electrochemical characteristics of the membrane electrode assembly when designing a proton exchange membrane fuel cell stack. *Electrochim. Acta*, **56**, 10406–10423.
22 Prater, K. (1990) The renaissance of the solid polymer fuel cell. *J. Power Sources*, **29**, 239–250.
23 Lim, C. and Wang, C.Y. (2004) Effects of hydrophobic polymer content in GDL on power performance of a PEM fuel cell. *Electrochim. Acta*, **49**, 4149–4156.
24 Sharaf, O.Z. and Orhan, M.F. (2014) An overview of fuel cell technology: fundamentals and applications. *Renew. Sustain. Energy Rev.*, **32**, 810–853.
25 Wang, Y., Chen, K.S., Mishler, J., Cho, S.C., and Adroher, X.C. (2011) A review of polymer electrolyte membrane fuel cells: technology, applications, and needs on fundamental research. *Appl. Energy*, **88**, 981–1007.
26 Li, X. and Faghri, A. (2013) Review and advances of direct methanol fuel cells (DMFCs) part I: design, fabrication, and testing with high concentration methanol solutions. *J. Power Sources*, **226**, 223–240.
27 Hochgraf, C. (2009) Application of fuel cells in transportation: electric vehicles, in *Encyclopedia of Electrochemical Power Sources* (ed J. Garche), Elsevier, Amsterdam, pp. 236–248.
28 Pollet, B.G., Staffell, I., and Shang, J.L. (2012) Current status of hybrid, battery and fuel cell electric vehicles: from electrochemistry to market prospects. *Electrochim. Acta*, **84**, 235–249.
29 Eberle, U., Müller, B., and Von Helmolt, R. (2012) Fuel cell electric vehicles and hydrogen infrastructure: status 2012. *Energy Environ. Sci.*, **5**, 8780–8798.
30 Hamnett, A. (2003) Direct methanol fuel cells (DMFC), in *Handbook of Fuel Cells: Fundamentals and Survey of Systems*, vol. 1 (eds W. Vielstich, A. Lamm, and H. Gasteiger), John Wiley & Sons, Ltd, Chichester, Chapter 18, pp. 305–322.
31 Coutanceau, C., Rakotondrainibe, A.F., Lima, A., Garnier, E., Pronier, S., Léger, J.-M., and Lamy, C. (2004) Preparation of Pt-Ru bimetallic anodes by galvanostatic pulse electrodeposition: characterization and application to the direct methanol fuel cell. *J. Appl. Electrochem.*, **34**, 61–66.
32 Han, J. and Park, E.-S. (2002) Direct methanol fuel-cell combined with a small back-up battery. *J. Power Sources*, **112**, 477–483.
33 http://ballard.com/
34 Li, Q., Jensen, J.O., Savinell, R.F., and Bjerrum, N.J. (2009) High temperature proton exchange membranes based on polybenzimidazoles for fuel cells. *Prog. Polym. Sci.*, **34**, 449–477.
35 http://worldwide.hyundai.com/WW/Showroom/Eco/ix35-Fuel-Cell/PIP/index.html.
36 http://www.toyota.fr/world-of-toyota/articles-news-events/2014/toyota-mirai.json.
37 https://www.mbusa.com/vcm/MB/DigitalAssets/pdfmb/fcell/248x168_b-klasse_f-cell_NP11_EN_DS_low2.pdf.